

5.0 Some Frontiers

In this final chapter of the book are gathered together imaging concepts that have been published, but have not yet come into routine industrial use. The first part of this chapter develops the mathematical concept of linear moveout and how it relates to velocity analysis. Data can be focused so that the interval velocity can be read directly. The latter part of the chapter is about multiple reflections. Here too linear moveout helps to define the problem. You will see basic mathematical tools that have the power to deal with multiple reflections and lateral velocity variations. This chapter has many data processing proposals. They are not descriptions of production processes!

Interpreting Seismic Data

Initially I regarded this chapter as one for specialists interested mainly in devising new processes. Then I realized that in dealing with things that don't seem to work as they are expected to, we are really, for the first time, struggling to contend with reality, not with what theory predicts. This can hold much interest for skilled interpreters.

The heart of petroleum prospecting is the interpretation of reflection seismic data. What is seismic interpretation? To be a "routine interpreter" you must know everything on which theory and practice generally agree. To be a *good* interpreter you must know the "noise level" of alternate phenomena with similar effects. Anomalies in seismic data can arise from the complexity of the earth itself, from seismic wave propagation in the earth (deep, near surface, or out of plane), or from imperfections in recording and imaging techniques. To make realistic judgements in so wide a realm, you must be a seismologist who is part geologist, part engineer, and part mathematician. This chapter will not teach you to be a good interpreter, but it will offer you a chance to observe some critical thinking about the relationship of seismic theory to seismic data.

Leaning

Echo delay is much like depth. We usually measure angles by their departure from the *vertical* ray, while in reality zero-offset data is rarely recorded. The best seismic data is usually far from vertical. In this chapter a pattern of thinking is developed that is oriented about a selected nonvertical ray. Rotation of coordinates does not solve the problem since after rotation, the plane on which measurements would be made would no longer be simply $z = 0$. Rotation would also make a mess of the simple seismic velocity function $v(z)$ by making it a strongly two-dimensional function $v'(x', z')$. The view of offset presented in Chapter 3 may have seemed rather complete, but in fact it was not very general because square roots were expanded about the vertical ray. The Stolt stretch development in Section 4.5 illustrated the advantage of leaving the hyperbola top and getting out on the flanks.

Linear moveout (LMO) is the way to reorient our thinking about nonvertical rays. While not widely incorporated in the modern production environment, this deeper view of offset is of special interest to researchers. It offers an understanding of multiple reflections, a subject untouched in Chapter 3. It also offers a better understanding of velocity estimation.

Stepout Review

In Section 1.5 a *Snell wave* was defined as a plane wave that has become nonplanar by moving into a velocity-stratified medium $v = v(z)$. A plane wave keeps its angle of propagation constant, while a Snell wave keeps its stepout dt/dx a constant function of z . Figure 1 shows a Snell wave incident on the earth's surface. The wavefronts at successive times are not parallel to each other; they are horizontal translations of one another. The *slowness* of horizontal motion is called the *stepout*. It is measured in units of inverse velocity and is given as milliseconds per meter or as seconds per kilometer. The slowness, denoted as p , is also called the *ray parameter* or the *Snell parameter*:

$$p = \frac{dt}{dx} = \frac{\sin \theta(z)}{v(z)} = \text{const}(z) \quad (1)$$

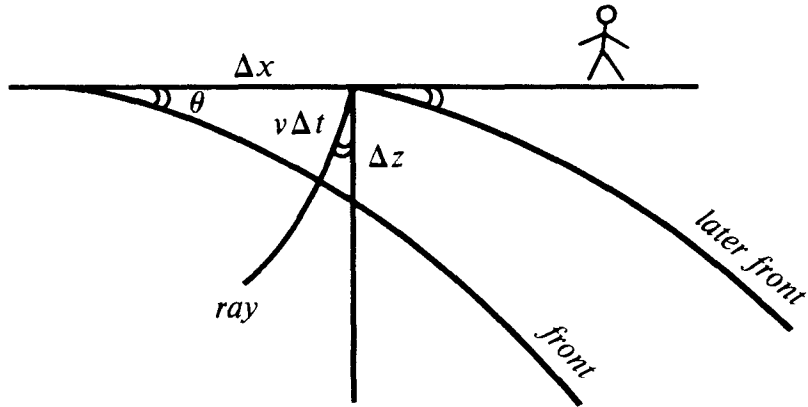


FIG. 5.0-1. Wavefront arrival at earth's surface, showing that observation of dt/dx gives the ratio $dt/dx = (\sin \theta)/v$.

5.1 Radial Traces

Radial trace sections were introduced in Section 3.6 as an alternative to constant-offset sections. In Section 3.6 the goal was to achieve a proper migration of nonzero-offset data. We also saw the definition of dip moveout (DMO). DMO simplifies further analysis because after DMO we can analyze gathers assuming that they come from a horizontally layered earth.

A *radial trace gather* is defined by a deformation of an ordinary gather. Let the ordinary gather be denoted by $P(x, t)$. Let the radial parameter be denoted by $r = x/t$. Then the radial trace gather $P'(r, t)$ is defined by the deformation $P'(r, t) = P(rt, t)$.

The horizontal location x of the tip of a ray moves according to $x = v t \sin \theta$. So in a constant-velocity medium, the radial trace with a fixed $r = x/t$ contains all the energy that propagates at angle θ .

The constancy of propagation angle within a radial trace should be helpful in the analysis of multiple reflections. It should also be helpful in compensation for the shot waveform, since the antenna effects of the shot and geophone arrays are time-invariant on each radial trace.

Assuming reflectors at depth z_j and constant velocity, hyperbolic travel-time curves are

$$t^2 v^2 = x^2 + z_j^2 \quad (1)$$

Let us see what happens to the hyperbola (1) when the offset x is transformed to the radial parameter $r = x/t$. We get an equation for a family of curves in the (r, t) -plane (plotted in figure 1).

$$z_j^2 = t^2 (v^2 - r^2) \quad (2)$$

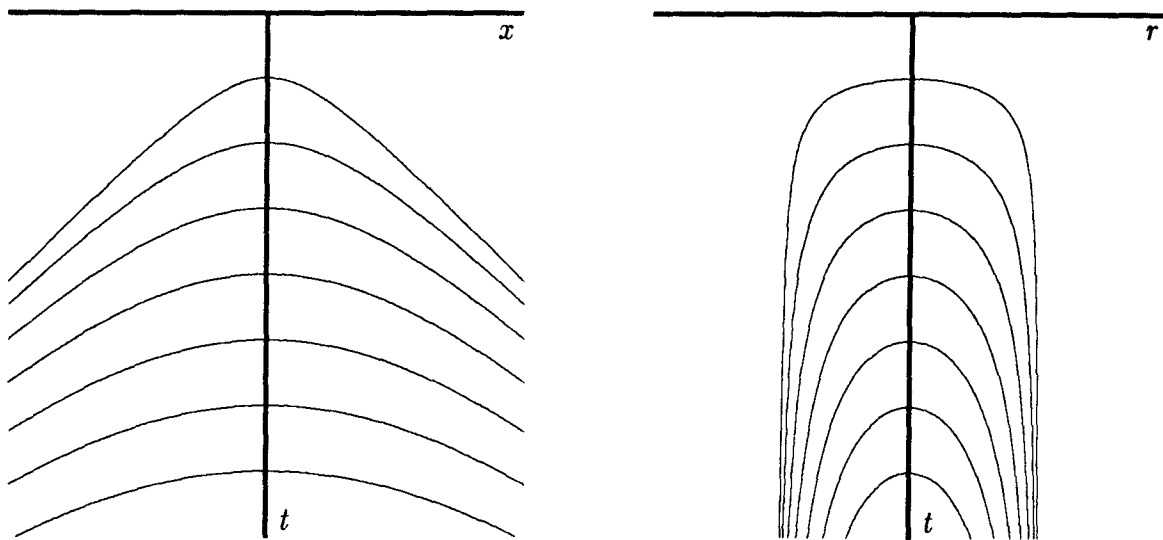


FIG. 5.1-1. Family of hyperbolas before and after transformation to radial space.

The asymptotes, instead of being along sloping lines $x^2 = \pm v^2 t^2$, are along vertical lines $r = \pm v$. The filled region of the (r, t) -plane is rectangular, while the filled region of the (x, t) -plane is triangular.

Figure 2 shows a field profile before and after transformation to radial space. Zero traces were interspersed between live ones to clarify the shape of the deformation. To understand this deformation, it helps to remember that a field trace is a curve of constant $x = rt$.

An interesting aspect of the radial-trace transformation is its effect on ground roll. A simple model of ground roll is a wave traveling horizontally at a constant rate. So on a radial-trace gather the ground roll is found as d.c. (zero frequency) on a few radial traces near $r = \pm v_{roll}$. Figure 3 shows an approximation to the idealization.

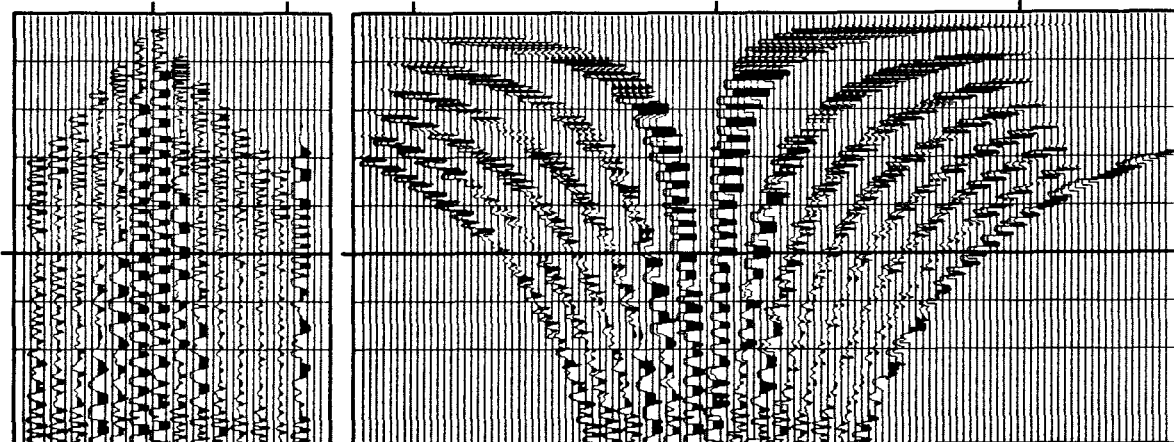


FIG. 5.1-2. Field profile from Alberta (Western Geophysical) interspersed with zero traces, shown before and after radial-trace deformation.

Moveout-Corrected Radial Traces

Moveout correction may be regarded as a transformation from time to depth. When the moveout correction is properly done, all traces should show the same depth-dependent reflectivity. In principle, radial moveout correction proceeds by introducing z and eliminating t with the substitution $tv = \sqrt{z^2+x^2}$. In practice you would prefer a travel-time-depth axis to a depth axis. So the transformation equation becomes $t = \sqrt{r^2+x^2/v^2}$. Eliminating x with rt we get

$$t = \frac{\tau}{\sqrt{1 - r^2/v^2}} \quad (3)$$

Inspecting (3) we see that moveout correction in radial-trace coordinates is a *uniform compression* of the time t -axis into a τ -axis. The amount of compression is fixed when r is fixed. The amount of compression does not change with time. The uniformity of the compression is an aid to modeling and removing the effects of shot waveforms and multiple reflections. It is curious to note that moveout correction of radial traces *compresses* time, while moveout correction of constant-offset data *stretches* time nonuniformly. Figure 3 shows a field profile before and after the radial-trace transformation.

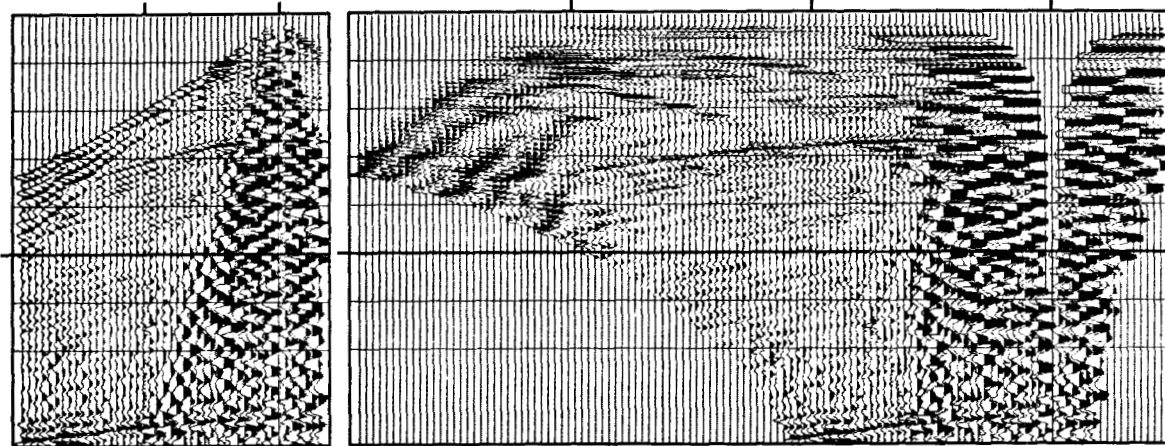


FIG. 5.1-3. Field profile from Alberta (Western Geophysical) shown before and after deformation into radial traces.

Snell Traces

The radial-trace coordinate system can be used no matter what the velocity of the earth. But the coordinate system has a special advantage when the velocity is constant, because then it gathers all the energy of a fixed propagation angle. The logical generalization to stratified media is to gather all the energy with a fixed Snell parameter. A *Snell trace* is defined (Ottolini) as a trajectory on the (x, t) -plane where the stepout $p = dt/dx$ would be constant if the velocity were $v(z)$. Where the velocity increases with depth, the Snell trace trajectory is readily found by integrating the ray equations:

$$x = \int_0^z \tan \theta \, dz \quad (4a)$$

$$t = \int_0^z \frac{dz}{v \cos \theta} \quad (4b)$$

To do moveout correction on the Snell traces, introduce the vertical travel-time depth τ such that $dz = v \, d\tau$. The radial-trace moveout-correction equations become

$$x(p, \tau) = \int_0^\tau \frac{p v^2}{\sqrt{1-p^2 v^2}} \, d\tau \quad (5a)$$

$$t(p, \tau) = \int_0^\tau \frac{1}{\sqrt{1-p^2 v^2}} \, d\tau \quad (5b)$$

Where the earth velocity is stratified, Snell traces have a theoretical advantage over radial traces. However they have the disadvantage that the curves could become multibranched, so that the transformation would not be one-to-one. So in practice you might use a simplified velocity model instead of your best estimate of the true velocity.

More philosophically, the transition from constant-offset traces to radial traces is a big one, whereas the transition from radial traces to Snell traces is not so large. Since the use of radial traces is not widespread, we can speculate that the practical usefulness of Snell traces may be further limited.

5.2 Slant Stack

Slant stack is a transformation of the offset axis. It is like steering a beam of seismic waves. I believe I introduced the term *slant stack* (Schultz and Claerbout [1978]) as a part of a migration method to be described next in Section 5.3. I certainly didn't invent the slant-stack concept! It has a long history in exploration seismology going back to Professor Rieber in the 1930s and to Professor Riabinkin in the Soviet Union. Mathematically, the slant-stack concept is found in the Radon [1917] transformation.

The slant-stack idea resembles the Snell trace method of organizing data around emergent angle. The Snell trace idea selects data based on a hypothetical velocity predicting the local stepout $p = dt/dx$. Slant stack does not *predict* the stepout, but *extracts* it by filtering. Thus slant stack does its job correctly whether or not the velocity is known. When the velocity of the medium is known, slant stack enables immediate downward continuation even when mixed apparent velocities are present as with diffractions and multiple reflections.

Slant Stacking and Linear Moveout

Looking on profiles or gathers for events of some particular stepout $p = dt/dx$ amounts to scanning hyperbolic events to find the places where they are tangent to a straight line of slope p . The search and analysis will be easier if the data is replotted with *linear moveout* — that is, if energy located at offset $x = g - s$ and time t in the (x, t) -plane is moved to time $\tau = t - px$ in the (x, τ) -plane. This process is depicted in figure 1. The linear moveout converts all events stepping out at a rate p in (x, t) -space to “horizontal” events in (x, τ) -space. The presence of horizontal timing lines facilitates the search for and the identification and measurement of the locations of the events.

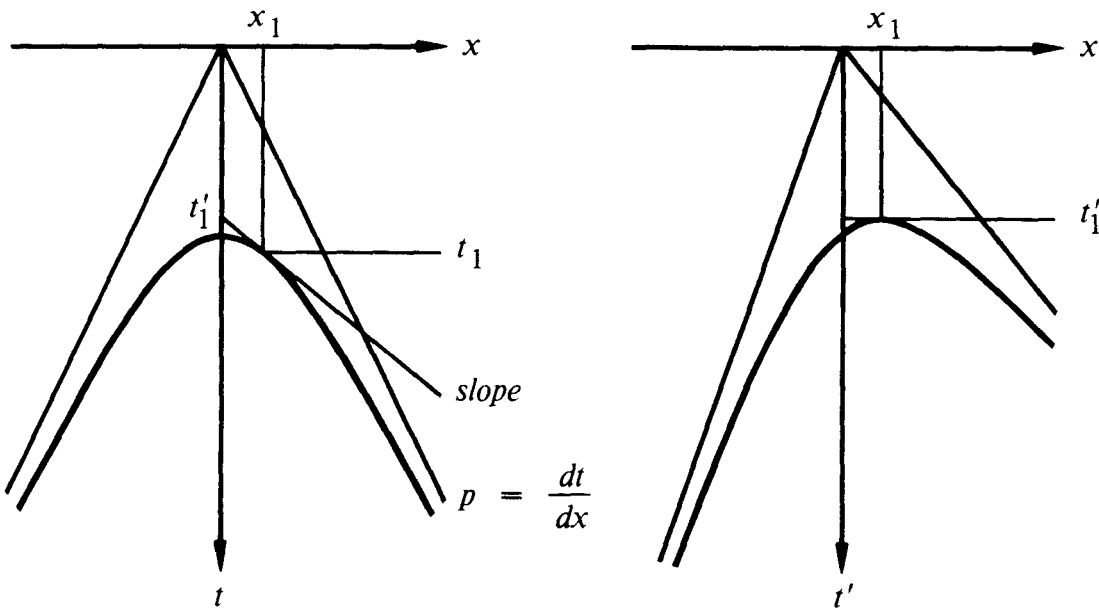


FIG. 5.2-1. Linear moveout converts the task of identifying tangencies to constructed parallel lines to the task of locating the tops of convex events.

After linear moveout $\tau = t - px$, the components in the data that have Snell parameters near p are slowly variable along the x -axis. To extract them, apply a low-pass filter on the x -axis, and do so for each value of τ . The limiting case of low-frequency filtering is extracting the mean. This leads to the idea of slant stack.

To *slant stack*, do linear moveout with $\tau = t - px$, then sum over x . This is the same as summing along slanted lines in (t, x) -space. In either case, the entire gather $P(x, t)$ gets converted to a single trace that is a

function of τ .

Slant stack assumes that the sum over observed offsets is an adequate representation of integration over all offset. The (slanted) integral over offset will receive its major contribution from the zone in which the path of integration becomes tangent to the hyperboloidal arrivals. On the other hand, the contribution to the integral is vanishingly small when the arrival-time curve crosses the integration curve. The reason is that propagating waves have no zero-frequency component.

The strength of an arrival depends on the length of the zone of tangency. The Fresnel definition of the length of the zone of tangency is based on a half-wavelength condition. In an earth of constant velocity (but many flat layers) the width of the tangency zone would broaden with time as the hyperbolas flatten. This increase goes as \sqrt{t} , which accounts for half the spherical-divergence correction. In other words, slant stacking takes us from two dimensions to one, but a \sqrt{t} remains to correct the conical wavefront of three dimensions to the plane wave of two.

Slant-Stack Gathers are Ellipses.

A slant stack of a data gather yields a single trace characterized by the slant parameter p . Slant stacking at many p -values yields a *slant-stack gather*. (Those with a strong mathematical-physics background will note that slant stacking transforms travel-time curves by the Legendre transformation. Especially clear background reading is found in *Thermodynamics*, by H.B. Callen, Wiley, 1960, pp. 90-95).

Let us see what happens to the familiar family of hyperbolas $t^2v^2 = z_j^2 + x^2$ when we slant stack. It will be convenient to consider the circle and hyperbola equations in *parametric* form, that is, instead of $t^2v^2 = x^2 + z^2$, we use $z = vt \cos \theta$ and $x = vt \sin \theta$ or $x = z \tan \theta$. Take the equation for linear moveout

$$\tau = t - p x \quad (1)$$

and eliminate t and x with the parametric equations.

$$\tau = \frac{z}{v \cos \theta} - \frac{\sin \theta}{v} z \tan \theta = \frac{z}{v} \cos \theta \quad (2)$$

$$\tau = \frac{z}{v} \sqrt{1 - p^2 v^2} \quad (3)$$

Squaring gives the familiar ellipse equation

$$\left(\frac{\tau}{z} \right)^2 + p^2 = \frac{1}{v^2} \quad (4)$$

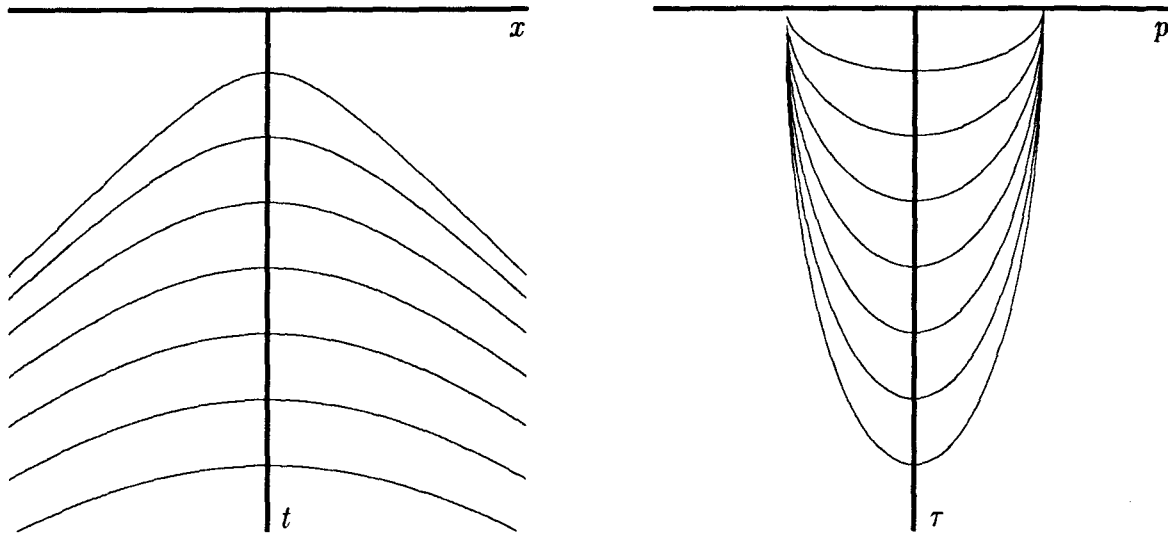


FIG. 5.2-2. Travel-time curves for a data gather on a multilayer earth model of constant velocity before and after slant stacking.

Equation (4) is plotted in figure 2 for various reflector depths z_j .

Two-Layer Model

Figure 3 shows the travel times of waves in a two-layer model. As is the usual case, the velocity is higher in the deeper layer. At the left are the familiar hyperboloidal curves. Strictly, the top curve is exactly a hyperbola whereas the lower curve is merely hyperboloidal. The straight line through the origin represents energy traveling horizontally along the earth's surface. The lower straight line is the head wave. (In seismology it is often called the *refracted* wave, but this name can cause confusion). It represents a ray that hits the deeper layer at critical angle and then propagates horizontally along the interface.

The right side of the figure shows the travel-time curves after slant stacking. Note that curves cross one another in the (x, t) -space but they do not cross one another in the (p, τ) -space. The horizontal axis $p = dt/dx$ has physical dimensions inverse to velocity. Indeed, the velocity of each layer may be read from its travel-time curve as the maximum p -value on its ellipse. The head waves — which are straight lines in (x, t) -space — are points in (p, τ) -space located where the ellipsoids touch. The top curve in (p, τ) -space is exactly an ellipse, and the lower curve is merely ellipsoidal.

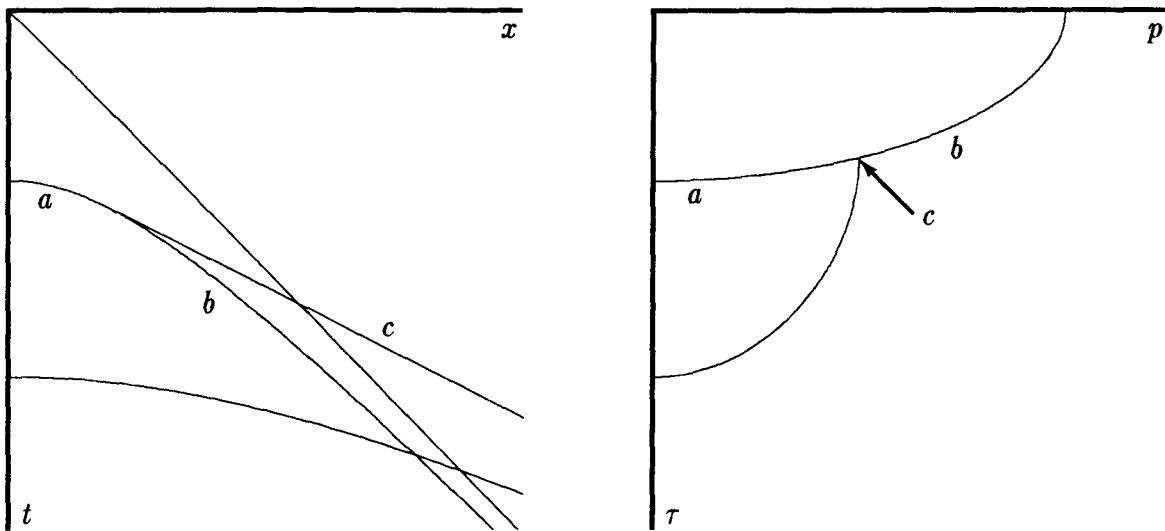


FIG. 5.2-3. Identification of precritical reflection (a), postcritical reflection (b), and head wave (c).

Interval Velocities from Slant Stacks

Section 1.5 showed that downward continuation of Snell waves is purely a matter of time shift. The amount of time shift depends only on the angle of the waves. For example, a frequency domain equation for the shifting is

$$P(\omega, p, z_2) = P(\omega, p, z_1) e^{-i \frac{\omega}{v} \sqrt{1 - p^2 v^2} (z_2 - z_1)} \quad (5)$$

Downward continuing to the first reflector, we find that the first reflections should arrive at zero time. In migration it is customary to retard time with respect to the zero-dip ray. So downward continuation in retarded time flattens the first reflection without changing the zero-dip ray. Time shifting the data to align on the first-layer reflection is illustrated by the third panel in figure 4. The first panel shows the velocity model, and the second panel shows the slant stacks at the surface. After the first reflector is time aligned, we have the data that should be observed at the bottom of the first layer. Now the next deeper curve is an exact ellipse. Estimate the next deeper velocity from that next deeper ellipse. Continue the procedure to all depths. This method of velocity estimation was proposed and tested by P. Schultz [1982].

Figure 4 illustrates the difficulty caused by a shallow, high-velocity layer. Reflection from the bottom of any deeper, lower-velocity layer gives an incomplete ellipse. It does not connect to the ellipse above because it seems to want

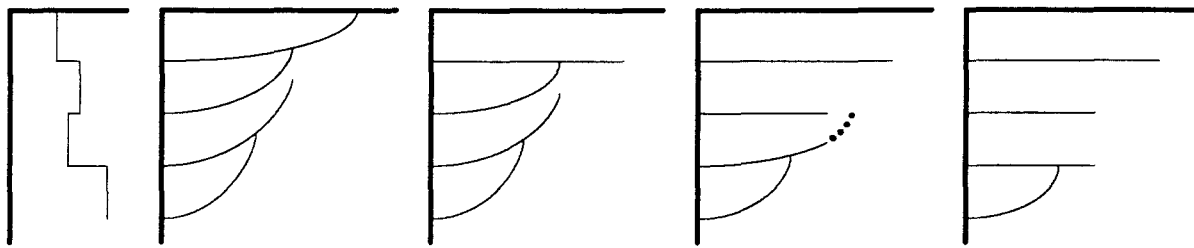


FIG. 5.2-4. Schultz flattening on successive layers.

to extend beyond. The large p -values (dotted in the figure) are missing because they are blocked by the high-velocity (low p) layer above. The cutoff in p happens where waves in the high-velocity layer go horizontally. So there are no head waves on deeper, lower-velocity layer bottoms.

Schultz's method of estimating velocity from an ellipse proceeds by summing on scanning ellipses of various velocities and selecting the one with the most power. So his method should not be troubled by shallow high-velocity layers. It is interesting to note that when the velocity does increase continuously with depth, the velocity-depth curve can be read directly from the rightmost panel of figure 4. The velocity-depth curve would be the line connecting the ends (maximum p) of the reflections, i.e. the head waves.

Interface Velocity from Head Waves

The determination of earth velocity from head waves is an old subject in seismology. Velocity measurement from head waves, where it is possible, refers to a specific depth —the depth of the interface— so it has even better depth-resolving power than an *interval* velocity (the velocity of a depth interval between two reflections).

Traditionally, head-wave velocity analysis involved identification (picking) of travel times. Travel times are hard to pick out on noisy data. Clayton and McMechan [1981] introduced a new method based on the wavefield itself, instead of on picked travel times. They did for the velocity analysis of head waves what wave-equation migration did for reflections.

The same idea for getting velocity from back-scattered head waves on sections (Section 3.5) can be used on ordinary head waves on common-midpoint gathers. On gathers you have the extra information not on a section that downward continuation focuses energy on zero offset. The focus is not a featureless point. Take original data to consist of a head wave only, with no reflection. Downward continuation yields a focus at zero offset. The

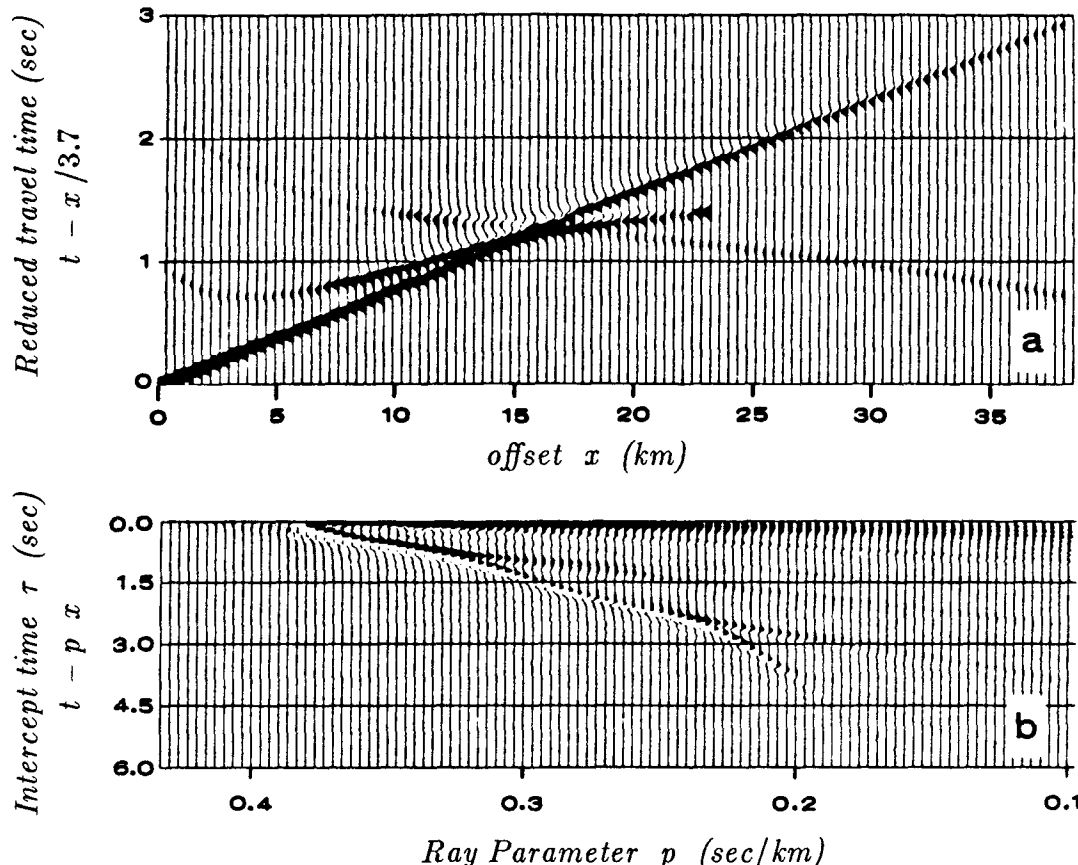


FIG. 5.2-5. The upper figure (a) contains a synthetic head-wave profile (plotted with linear moveout). The data is transformed by slant stack to the lower half of the figure (b). The result of downward continuation of this slant-stacked wavefield (b) is shown in figure 6. (Clayton & McMechan)

focus is a concentrated patch of energy oriented with the same stepout dt/dh as the original unfocused head wave. Summing through the focus at all possible orientations (slant stack) transforms the data $u(h, \tau)$ to dip space, say $\bar{u}(p, \tau)$. The velocity of the earth at travel-time depth τ is found where the seismic energy has concentrated on the (p, τ) -plane. The velocity is given directly by $v(\tau) = 1/p(\tau)$. Given $v(\tau)$, $v(z)$ is readily found. Or the entire calculation could be done in depth z directly instead of in travel-time depth τ .

Clayton and McMechan actually do the downward continuation and the slant stack in the opposite order. They slant stack first and then downward continue. In principle these processes can be done in either order. Remember that we are bootstrapping to the correct earth velocity. Slant stacking does

not depend on the earth's velocity, but downward continuation does. Slant stacking need be done only once if it is done first, which is why Clayton and McMechan do it that way. Figures 5 and 6 show one of their examples.

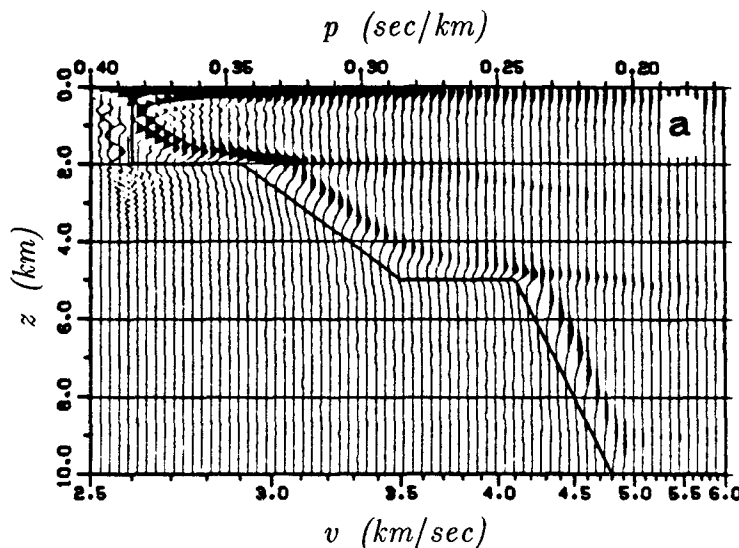


FIG. 5.2-6. The result of downward continuation of the slant-stacked wavefield in figure 5b with the correct velocity-depth function (the solid line). (Clayton & McMechan)

Compare the method of Clayton and McMechan to that of Schultz. Schultz flattens the reflections by a method that is sensitive to the large p parts of the ellipse. Clayton and McMechan look only at the largest p part of the ellipse. Schultz has the advantage that a method based on reflection is not troubled by high-velocity layers, but the disadvantage that decision making is required during the descent. Clayton and McMechan present the interpreter with a plane of information from which the interpreter selects the velocity. Clayton and McMechan's velocity space is a linear, invertible function of the data. Section 5.4 will describe a linear, invertible transformation of *reflection* data (not head waves) to velocity space.

Slant Stack and Fourier Transform

Let $u(x, t)$ be a wavefield. The *slant stack* $\bar{u}(p, \tau)$ of the wavefield is defined mathematically by

$$\boxed{\bar{u}(p, \tau) = \int u(x, \tau + px) dx} \quad (6)$$

The integral across x in (6) is done at constant τ , which is a slanting line in the (x, t) -plane.

Slant stack is readily expressed in Fourier space. The definition of the two-dimensional Fourier transformation of the wavefield $u(x, t)$ is

$$U(k, \omega) = \iint e^{i\omega t - ikx} u(x, t) dx dt \quad (7)$$

Recall the definition of Snell's parameter in Fourier space $p = k/\omega$ and use it to eliminate k from the 2-D Fourier transform (7).

$$U(\omega p, \omega) = \iint e^{i\omega(t - px)} u(x, t) dx dt \quad (8)$$

Change the integration variable from t to $\tau = t - px$.

$$U(\omega p, \omega) = \int e^{i\omega\tau} [\int u(x, \tau + px) dx] d\tau \quad (9)$$

Insert the definition (6) into (9).

$$U(\omega p, \omega) = \int e^{i\omega\tau} \bar{u}(p, \tau) d\tau \quad (10)$$

Think of $U(\omega p, \omega)$ as a one-dimensional function of ω that is extracted from the (k, ω) -plane along the line $k = \omega p$.

The inverse Fourier transform of (10) is

$$\boxed{\bar{u}(p, \tau) = \int e^{-i\omega\tau} U(\omega p, \omega) d\omega} \quad (11)$$

The result (11) states that a slant stack can be created by Fourier-domain operations. First you transform $u(x, t)$ to $U(k, \omega)$. Then extract $U(\omega p, \omega)$ from $U(k, \omega)$. Finally, inverse transform from ω to τ and repeat the process for all interesting values of p .

Getting $U(\omega p, \omega)$ from $U(k, \omega)$ seems easy, but this turns out to be the hard part. The line $k = \omega p$ will not pass nicely through all the mesh points (unless $p = \Delta t / \Delta x$) so some interpolation must be done. As we have seen from the computational artifacts of Stolt migration, Fourier-domain interpolation should not be done casually. Interpolation advice is found in

Section 4.5.

Both (6) and (11) are used in practice. In (6) you have better control of truncation and aliasing. For large datasets, (11) is much faster.

Inverse Slant Stack

Tomography in medical imaging is based on the same mathematics as inverse slant stack. Simply stated, (two-dimensional) tomography or inverse slant stacking is the reconstruction of a function given line integrals through it. The inverse slant-stack formula will follow from the definition of two-dimensional Fourier integration:

$$u(x, t) = \int e^{-i\omega t} \left[\int e^{ikx} U(k, \omega) dk \right] d\omega \quad (12)$$

Substitute $k = \omega p$ and $dk = \omega dp$ into (12). Notice that when ω is negative the integration with dp runs from positive to negative instead of the reverse. To keep the integration in the conventional sense of negative to positive, introduce the absolute value $|\omega|$. (More generally, a change of variable of volume integrals introduces the *Jacobian* of the transformation). Thus,

$$u(x, t) = \int e^{-i\omega t} \left[\int e^{i\omega px} U(\omega p, \omega) |\omega| dp \right] d\omega \quad (13)$$

$$u(x, t) = \int \left\{ \int e^{-i\omega t} [U(\omega p, \omega) e^{i\omega px} |\omega|] d\omega \right\} dp \quad (14)$$

Observe that the $\{ \}$ in (14) contain an inverse Fourier transform of a product of three functions of frequency. The product of three functions in the ω -domain is a convolution in the time domain. The three functions are first $U(\omega p, \omega)$, which by (11) is the FT of the slant stack. Second is a delay operator $e^{i\omega px}$, i.e an impulse function of time at time px . Third is an $|\omega|$ filter. The $|\omega|$ filter is called a *rho* filter. The *rho* filter does not depend on p so we may separate it from the integration over p . Let “ $*$ ” denote convolution. Introduce the delay px as an argument shift. Finally we have the inverse slant-stack equation we have been seeking:

$$u(x, t) = \text{rho}(t) * \int \bar{u}(p, t-px) dp \quad (15)$$

It is curious that the inverse to the slant-stack operation (6) is basically another slant-stacking operation (15) with a sign change.

Plane-Wave Superposition

Equation (15) can be simply interpreted as plane-wave superposition. To make this clear, we first dispose of the *rho* filter by means of a definition.

$$\tilde{u}(p, \tau) = \text{rho}(\tau) * \bar{u}(p, \tau) \quad (16)$$

Equation (16) will be seen to be more than a definition. We will see that $\tilde{u}(p, \tau)$ can be interpreted as the *plane-wave spectrum*. Substituting the definition (16) into both (15) and (6) gives another transform pair:

$u(x, t) = \int \tilde{u}(p, t - px) dp$	(17)
--	------

$\tilde{u}(p, \tau) = \text{rho}(\tau) * \int u(x, \tau + px) dx$	(18)
---	------

To confirm that $\tilde{u}(p, \tau)$ may be interpreted as the plane-wave spectrum, we take $\tilde{u}(p, \tau)$ to be the impulse function $\delta(p - p_0) \delta(\tau - \tau_0)$ and substitute it into (17). The result $u(x, t) = \delta(t - p_0 x - \tau_0)$ is an impulsive plane wave, as expected.

Reflection Coefficients — Spherical versus Planar

The amplitudes that you see on the reflected waves on a field profile are affected by many things. Assume that corrections can be made for the spherical divergence of the wave, the transmission coefficients through the layers, inner bed multiples, etc. What remains are the *spherical-wave reflection coefficients*. Spherical-wave reflection strengths are not the same as the plane-wave reflection coefficients calculated in FGDP or by means of Zoepfritz [1919] equations. Theoretical analyses of reflection coefficient strengths are always based on Fourier analysis. Equations (17) and (18) provide a link between plane-wave reflection coefficients and cylindrical-wave reflection coefficients. See page 196 for going from cylinders to spheres.

The Rho Filter

In practical work, the *rho* filter is often ignored because it can be absorbed into the rest of the filtering effects of the overall data recording and processing activity. However, the *rho* filter is not inconsequential. The integrations in the slant stack enhance low frequencies, and the *rho* filter pushes them back to their appropriate level. Let us inspect this filter. The *rho* filter has the same spectrum as does the time derivative, but their time functions are very different. The finite-difference representation of a time derivative is short, only Δt in time duration. Because of the sharp corner in the absolute-value function, the *rho* filter has a long time duration. The

Hilbert kernel $-1/t$ has a Fourier transform $i \operatorname{sgn}(\omega)$. Notice that $|\omega| = (-i\omega) \times i \operatorname{sgn}(\omega)$. In the time domain this means that $d/dt(-1/t) = 1/t^2$, so $\rho(t) = 1/t^2$.

An alternate view is that the ρ filter should be divided into two parts, with half going into the forward slant stack and the other half into the inverse. Then slant stacking would not cause the power spectrum of the data to change. An interesting way to divide the $|\omega|$ is $|\omega| = \sqrt{-i\omega} \sqrt{i\omega}$. It was shown in Section 4.6 that $\sqrt{-i\omega}$ is a causal time function and $\sqrt{i\omega}$ is anticausal. More details about slant stacks are found in Phinney et al. [1981].

In practice, slant stack is not so cleanly invertible as 2-D FT, so various iteration and optimization techniques are often used.

EXERCISES

1. Assume that $v(z) = \text{const}$ and prove that the width of a Fresnel zone increases in proportion to \sqrt{t} .
2. Given $v(z)$, derive the width of the Fresnel zone as a function of t .

5.3 Snell Waves and Skewed Coordinates

Slant stacks are closely related to Snell waves. But there is more to it than that. Three different types of gathers (CSP, CGP, and CMP) can be slant stacked, and the meaning is different in each case.

A Snell wave can be synthesized by slant stacking ordinary reflection data. Snell waves are described by wave-propagation theory. You can expect to be able to write a wave equation that really describes the Snell wave despite complexities of lateral velocity variation, multiple reflections, shear waves, or all these complications at once. Contrast this to a CDP stack where downward continuation is already an approximation even when velocity

is constant. Of course we can always return to data analysis in shot-geophone space. But the slant stack is a stack, and that means there is already some noise reduction and data compression.

Snell Wave Information in Field Data

The superposition principle allows us to create an impulse function by a superposition of sinusoids of all frequencies. A three-dimensional generalization is the creation of a point source by the superposition of plane waves going in all directions. Likewise, a plane wave can be a superposition of many Huygens secondary point sources. A Snell wave can be simulated by an appropriate superposition, called a *slant stack*, of the point-source data recorded in exploration.

Imagine that all the shots in a seismic survey were shot off at the same time. The downgoing wave would be approximately a plane wave. (Let us ignore the reality that the world is 3-D and not 2-D). The data recorded from such an experiment could readily be simulated from conventional data simply by summing the data field $P(s, g, t)$ over all s . In each common-geophone profile the traces would be summed with no moveout correction.

To simulate a nonvertical Snell wave, successive shots must be delayed (to correspond to a supersonic airplane), according to some prescribed $p_s = dt/ds$.

What happens if data is summed over the geophone axis instead of the shot axis? The result is point-source experiments recorded by receiver antennas that have been highly tuned to receive vertically propagating waves. Time shifting the geophones before summation simulates a receiver antenna that records a Snell wave, say, $p_g = dt/dg$ upcoming at an angle $\sin \theta = p_g v$.

Integration over an axis is an extreme case of low-pass filtering over an axis. Between the two extremes of the point-source case and the plane-wave case is the case of directional senders and receivers.

The simple process of propagation spreads out a point disturbance to a place where, from a distance, the waves appear to be nearly plane waves or Snell waves. Little patches of data where arrivals appear to be planar can be analyzed as though they were Snell waves.

In summary, a *downgoing* Snell wave is achieved by dip filtering in *shot* space, whereas an *upcoming* Snell wave is achieved by dip filtering in *geophone* space.

Muting and Data Recording

The basic goal of muting is to remove horizontally moving energy. Such energy is unrelated to a deeper image. Typically muting is performed as described in Section 3.5 — that is, a weighting function zeroes data generally beyond some value of $(g-s)/t$. There is no question that muting removes much horizontally moving energy, but more can be done. Because of back-scattering, horizontally moving energy can often be found inside the mute zone. The way to get rid of it is to use a dip filter instead of a weighting function. Before modern high-density recording, slow moving noises were often aliased on the geophone cable, so dip filtering wasn't feasible. If the emergent angle isn't close enough to vertical, that is, if dt/dg isn't small enough, then the waves can't have come from the exploration target. On explosion data, filtering is not so easily applied in shot space as it is in geophone space because data is not very densely recorded in shot space. Don't fall into the trap of thinking that this dip filtering can be done on a common-*mid* point gather. Back-scattered ground roll has no moveout on a common-*midpoint* gather (see Section 3.2).

Marine water-bottom scatter is frequently so strong that it is poorly suppressed by conventional processing. In Section 3.2 we saw the reason: point scatterers imply hyperbolic arrivals, which have steep dip, hence they have the stacking velocities of sediment rather than water. What is needed are two dip filters — one to reject waves leaving the shots at nonpenetrating angles, and the other to reject waves arriving at the geophones at non-penetrating angles.

Present-day field arrays filter on the basis of spatial frequency k_x . More high-frequency energy would be left in the data if the recording equipment used dip (k/ω) filters instead of spatial-frequency k filters. The causal dip filters described in Section 2.5 might work nicely.

Synthesizing the Snell Wave Experiment

Let us synthesize a downgoing Snell wave with field data, then imagine how the upcoming wave will look and how it will carry to us information about the subsurface.

Slant stacking will take the survey line data $P(s, g, t)$, which is a function of shot location s , geophone location g , and travel time t , and sum over the shot dimension, thereby synthesizing the upcoming wave $U(g, t)$, which should have been recorded from a downgoing Snell wave. This should be the case even though there may be lateral velocity variation and multiple reflections.

The summation process is confusing because three different kinds of time are involved:

t = travel time in the point-source field experiments.

t' = $t - p(g - s)$ = interpretation time. The shallowest reflectors are seen just after $t' = 0$.

t_{pseudo} = time in the Snell pseudoexperiment with a moving source.

Time in the pseudoexperiment in a horizontally layered earth has the peculiar characteristic that the further you move out the geophone axis, the later the echoes will arrive. Transform directly from the field experiment time t to interpretation time t' by

$$t' = t_{pseudo} - p x = t - p(g - s) \quad (1)$$

Figure 1 depicts a downgoing Snell wave.

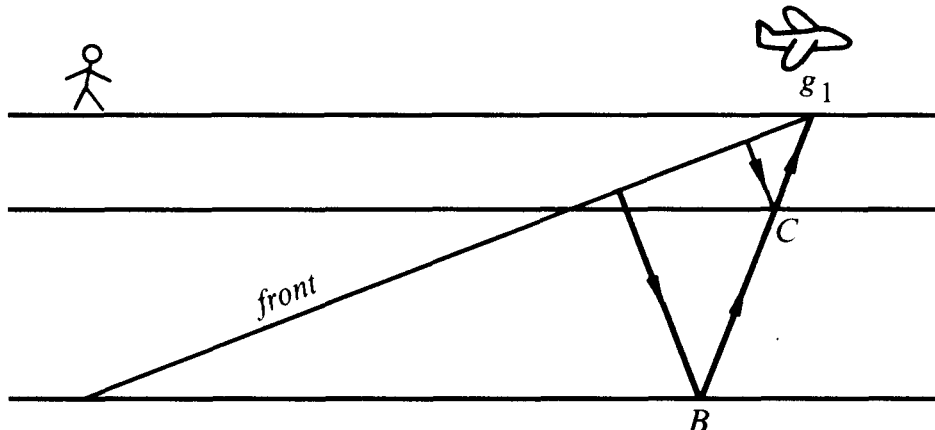


FIG. 5.3-1. Wavefront of a Snell wave that reflects from two layers, carrying information back up to g_1 .

Figure 2 shows a hypothetical common-geophone gather, which could be summed to simulate the Snell wave seen at location g_1 in figure 1. The lateral offset of B from C is identical in figure 1 with that in figure 2 (at two places in figure 2). Repeating the summation for all geophones synthesizes an upcoming wave from a downgoing Snell wave.

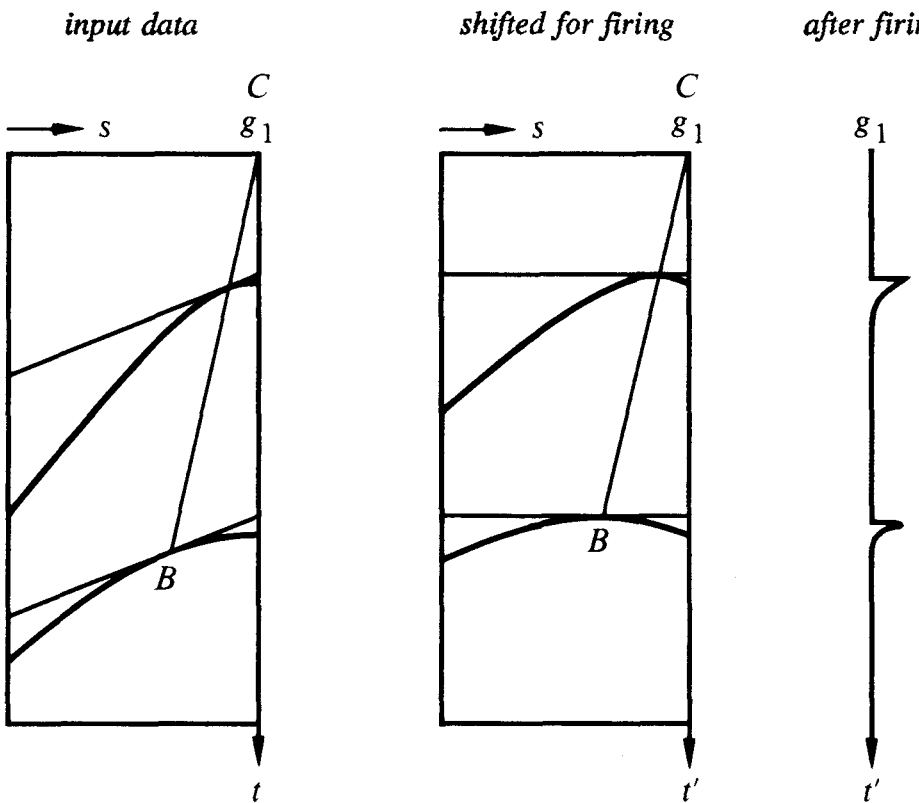


FIG. 5.3-2. On the left is a common-geophone gather at g_1 over two flat reflectors. In the center the data is shifted by linear moveout in preparation for the generation of the synthetic Snell wave by summation over shots. On the right is shown the Snell wave trace recorded at geophone g_1 . A Snell wave seismic section consists of many side-by-side traces like g_1 .

The variable t' may be called an interpretation coordinate, because shallow reflectors are seen just after $t' = 0$, and horizontal beds give echoes that arrive with no horizontal stepout, unlike the pseudo-Snell wave. For horizontal beds, the detection of lateral location depends upon lateral change in the reflection coefficient. In figure 1, the information about the reflection strength at B is recorded rightward at g_1 instead of being seen above B , where it would be on conventional stack. The moving of received data to an appropriate lateral location is thus an additional requirement for full interpretation.

Figure 3 shows the same two flat layers as figures 1 and 2, but there are also anomalous reflection coefficients at points A , B , and C . Point A is directly above point B . The path of the wave reflected at B leads directly to C and thence to g_1 . Subsequent frames show the diffraction hyperbolas associated with these three points. Notice that the pseudo-Snell waves

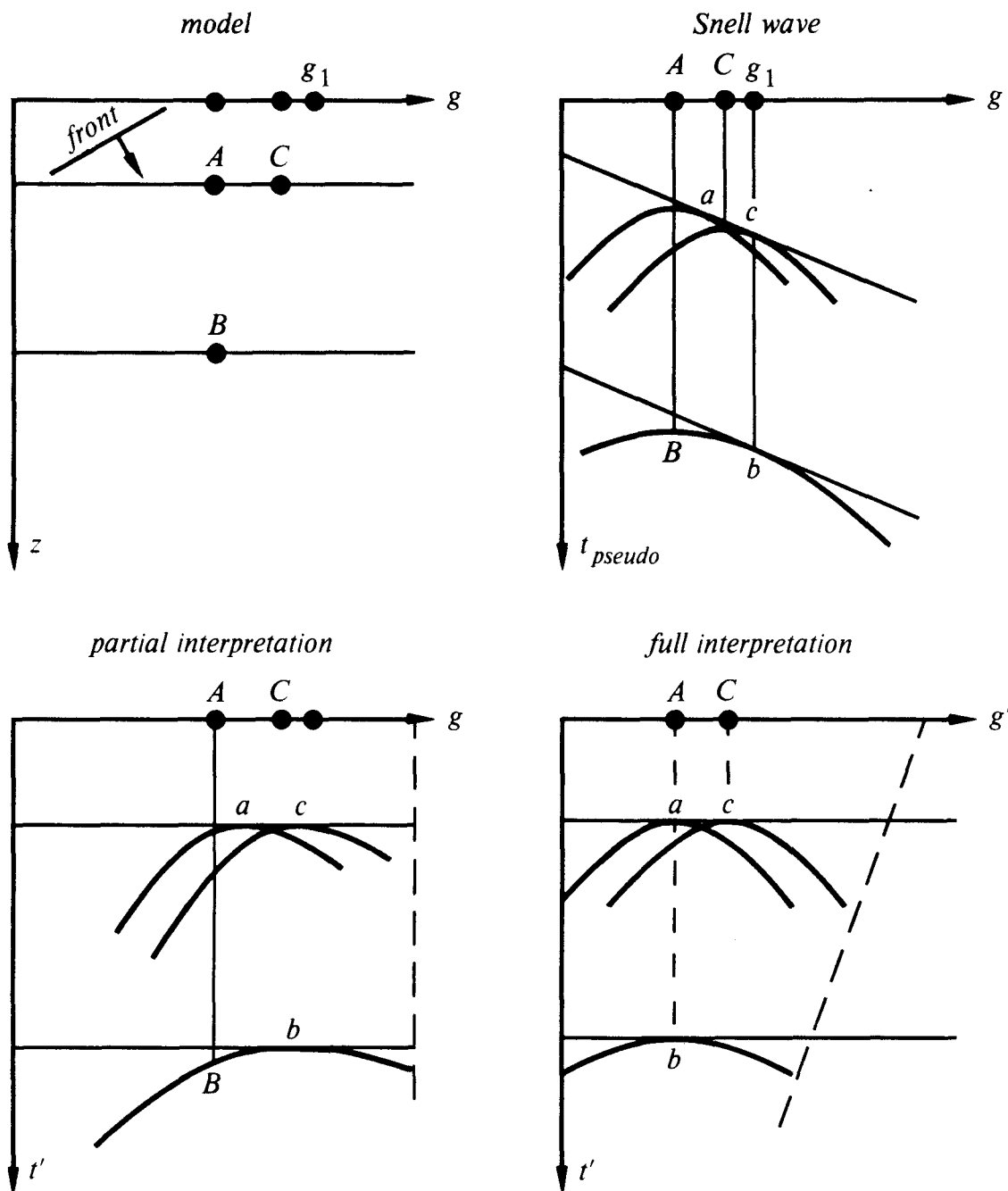


FIG. 5.3-3. Top left is three point scatterers on two reflectors. Top right is the expected Snell wave. Bottom left is the Snell wave after linear moveout. Bottom right is after transform to full interpretation coordinates. At last a , b , and c are located where A , B , and C began.

reflecting from the flat layers step out at a rate p . Hyperbolas from the scatters A , B , and C come tangent to the Snell waves at points a , b , and c . Notice that b and c lie directly under g_1 because all are aligned along a raypath with Snell parameter p . The points A , B , and C locate the tops of the hyperbolas since the earliest arrival must be directly above the point scatterer, no matter what the incident wavefield. Converting to the interpretation coordinate t' in the next frame offers the major advantage that arrivals from horizontal layers become horizontal. But notice that the hyperboloids have become skewed. Limiting our attention to the arrivals with little stepout, we find information about the anomalous reflection coefficients entirely in the vicinities of a , b , and c , which points originally lay on hyperbola flanks. These points will not have the correct geometrical location, namely that of A , B and C , until the data is laterally shifted to the left, to, say, $g' = g - f(t')$. Then a will lie above b . The correct amount of shift $f(t')$ is a subject that relates to velocity analysis. The velocity analysis that pertains to this problem will be worked out in the next section.

What's Wrong with Snell Waves?

Before the DSR was developed, I thought that the only proper way to analyze seismic data was to decompose it into Snell waves. Since a Fresnel zone seems to be about 10° wide, not many Snell waves should be required. The small number of required sections was important because of the limited power of computers in the 1970's. I knew that each Snell wave is analyzable by a single square-root equation, and that even multiple reflections can be handled by methods described in FGDP and here in Section 5.6. Theoretically this approach was a big improvement over CDP stack, which is hardly analyzable at all. A practical problem for downgoing Snell waves, however, is that they may become complicated early if they encounter lateral velocity inhomogeneity shortly after they depart the earth's surface. I no longer believe that Snell waves are a panacea, although I am unsure what their ultimate role will be. But many waves behave a little like they are Snell waves. This motivates the development of a coordinate system that is ideal for Snell waves, and good for waves that are not far from being Snell waves.

Lateral Invariance

The nice thing about a vertically incident source of plane waves $p = 0$ in a horizontally stratified medium is that the ensuing wavefield is laterally invariant. In other words, an observation or a theory for a wavefield would in this case be of the form $P(t) \times \text{const}(x)$. Snell waves for any particular nonzero p -value are also laterally invariant. That is, with

$$t' = t - p x \quad (2a)$$

$$x' = x \quad (2b)$$

lateral invariance is given by the statement

$$P(x, t) = P'(t') \times \text{const}(x') \quad (3)$$

Obviously, when an apparently two-dimensional problem can be reduced to one dimension, great conceptual advantages result, to say nothing of sampling and computational advantages. Before proceeding, study equation (3) until you realize why the wavefield can vary with x but be a constant function of x' when (2b) says $x = x'$.

The coordinate system (2) is a retarded coordinate system, not a moving coordinate system. Moving coordinate systems work out badly in solid-earth geophysics. The velocity function is never time-variable in the earth, but it becomes time-variable in a moving coordinate system. This adds a whole dimension to computational complexity.

The goal is to create images from data using a *model* velocity that is a function of all space dimensions. But the coordinate system used will have a *reference* velocity that is a function of depth only.

Snell Wave Coordinates

A Snell wave has three intrinsic planes, which suggests a coordinate system. First are the layer planes of constant z , which include the earth's surface. Second is the plane of rays. Third is the moving plane of the wave-front. The planes become curved when velocity varies with depth.

The following equations define *Snell wave coordinates*:

$$z'(z, x, t) = z \frac{\cos \theta}{v} \quad (4a)$$

$$x'(z, x, t) = z \tan \theta + x \quad (4b)$$

$$t'(z, x, t) = z \frac{\cos \theta}{v} - x \frac{\sin \theta}{v} + t \quad (4c)$$

Equation (4a) simply defines a travel-time depth using the vertical phase velocity seen in a borehole. Interfaces within the earth are just planes of constant z' .

Setting x' as defined by equation (4b) equal to a constant, say, x_0 , gives the equation of a ray, namely, $(x - x_0)/z = -\tan \theta$. Different values of x_0 are different rays.

Setting t' as defined by equation (4c) equal to a constant gives the equation for a moving wavefront. To see this, set $t' = t_0$ and note that at constant x you see the borehole speed, and at constant z you see the airplane speed.

Mathematically, one equation in three unknowns defines a plane. So, setting the left side of any of the equations (4a,b,c) to a constant gives an equation defining a plane in (z, x, t) -space. To get some practice, we will look at the intersection of two planes. Staying on a wavefront requires $dt' = 0$. Using equation (4c) gives

$$dt' = 0 = \frac{\cos \theta}{v} dz - \frac{\sin \theta}{v} dx + dt \quad (5)$$

Combining the constant wavefront equation $dt' = 0$ with the constant depth equation $dz' = dz = 0$ gives the familiar relationship

$$\frac{dt}{dx} = p \quad (6)$$

When coordinate planes are nonorthogonal, the coordinate system is said to be *affine*. With affine coordinates, such as (4), we have no problem with computational tractability, but we often do have a problem with our own confusion. For example, when we display movies of marine field data, we see a sequence of (h, t) -planes. Successive planes are successive shot points. So the data is displayed in (s, h) when we tend to think in the orthogonal coordinates (y, h) or (s, g) . With affine coordinates I find it easiest to forget about the coordinate axis, and think instead about the perpendicular plane. The shot axis s can be thought of as a plane of constant geophone, say, cg . So I think of the marine-data movie as being in (cs, ch, ct) -space. In this movie, another plane, really a family of planes, the planes of constant midpoints cy , sweep across the screen, along with the “texture” of the data (Section 3.0).

To define Snell coordinates when the velocity is depth-variable, it is only necessary to interpret (4) carefully. First, all angles must be expressed in terms of p by the Snell substitution $\sin \theta = p v(z)$. Then z must everywhere be replaced by the integral with respect to z .

Snell Waves in Fourier Space

The chain rule for partial differentiation says that

$$\begin{bmatrix} \partial_t \\ \partial_x \\ \partial_z \end{bmatrix} = \begin{bmatrix} t'_t & x'_t & z'_t \\ t'_x & x'_x & z'_x \\ t'_z & x'_z & z'_z \end{bmatrix} \begin{bmatrix} \partial_{t'} \\ \partial_{x'} \\ \partial_{z'} \end{bmatrix} \quad (7a,b,c)$$

In Fourier space, equations (7a) and (7b) may be interpreted as

$$-i\omega = -i\omega \quad (8a)$$

$$i k_x = +p\omega' + i k'_x \quad (8b)$$

Of particular interest is the energy that is flat after linear moveout (constant with x'). For such energy $\partial/\partial x' = i k'_x = 0$. Combining (8a) and (8b) gives the familiar equation

$$p = \frac{k}{\omega} \quad (9)$$

EXERCISES

1. Explain the choice of sign of the s -axis in figure 1.
2. Equation (4) is for *upgoing* Snell waves. What coordinate system would be appropriate for *downgoing* Snell waves?
3. Express the scalar wave equation in the coordinate system (4). Neglect first derivatives.
4. Express the dispersion relation of the scalar wave equation in terms of the Fourier variables (ω', k'_x, k'_z) .

5.4 Interval Velocity by Linear Moveout

Linear moveout forms the basis for a simple, graphical method for finding seismic velocity. The method is particularly useful for the analysis of data that is no longer in a computer, but just exists on a piece of paper. Additionally, the method offers insights beyond those offered by the usual computerized hyperbola scan. Using it will help us rid ourselves of the notion that angles should be measured from the vertical ray. Non-zero Snell parameter can be the “default.”

Ultimately this method leads to a definition of *velocity spectrum*, a plane in which the layout of data, after a linear invertible transformation, shows the seismic velocity.

Graphical Method for Interval Velocity Measurement

A wave of velocity v from a point source at location $(x, z) = (0, z_s)$ passes any point (x, z) at time t where

$$v^2 t^2 = x^2 + (z - z_s)^2 \quad (1)$$

In equation (1) x should be replaced by either half-offset h or midpoint y . Then t is two-way travel time; the velocity v is half the rock velocity; and $(z - z_s)$ is the distance to an image source.

Differentiating (1) with respect to t (at constant z) gives

$$v^2 2 t = 2 x \frac{dx}{dt} \quad (2)$$

$$v^2 = \frac{x}{t} \frac{dx}{dt} \quad (3)$$

Figure 1 shows that the three parameters required by (3) to compute the material velocity are readily measured on a common-midpoint gather.

Equation (3) can be used to estimate a velocity whether or not the earth really has a constant velocity. When the earth velocity is stratified, say, $v(z)$, it is easy to establish that the estimate (3) is exactly the root-mean-square (RMS) velocity. First recall that the bit of energy arriving at the point of tangency propagates throughout its entire trip with a constant Snell parameter $p = dt/dx$.

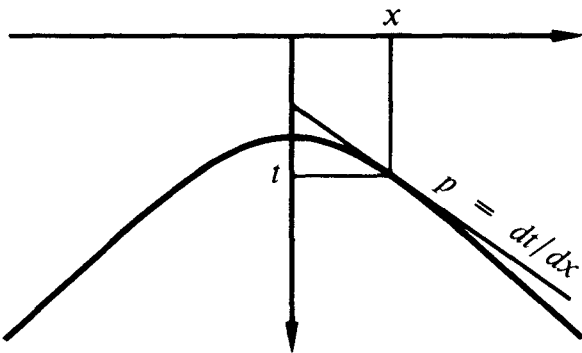


FIG. 5.4-1. A straight line, drawn tangent to hyperbolic observations. The slope p of the line is arbitrary and may be chosen so that the tangency occurs at a place where signal-to-noise ratio is good. (Gonzalez)

The best way to specify velocity in a stratified earth is to give it as some function $v'(z)$. Another way is to pick a Snell parameter p and start descending into the earth on a ray with this p . As the ray goes into the earth from the surface $z = 0$ at $t = 0$, the ray will be moving with a speed of, say, $v(p, t)$. It is an elementary exercise to compute $v(p, t)$ from $v'(z)$ and vice versa. The horizontal distance x which a ray will travel in time t is given by the time integral of the horizontal component of velocity, namely,

$$x = \int_0^t v(p, t) \sin \theta \, dt \quad (4)$$

Replacing $\sin \theta$ by pv and taking the constant p out of the integral yields

$$x = p \int_0^t v(p, t)^2 \, dt \quad (5)$$

Recalling that $p = dt/dx$, insert (5) into (3):

$$v_{\text{measured}}^2 = \frac{x}{t} \frac{dx}{dt} \quad (6)$$

$$v_{\text{measured}}^2 = \frac{1}{t} \int_0^t v(p, t)^2 \, dt \quad (7)$$

which justifies the assertion that

$$v_{\text{measured}} = v_{\text{root-mean-square}} = v_{\text{RMS}} \quad (8)$$

Equation (7) is exact. It does not involve a "small offset" assumption or a "straight ray" assumption.

Next compute the *interval* velocity. Figure 2 shows hyperboloidal arrivals from two flat layers. Two straight lines are constructed to have the same slope p . Then the tangencies are measured to have locations (x_1, t_1) and (x_2, t_2) . Combining (6) with (4), and using the subscript j to denote the j^{th} tangency (x_j, t_j) , gives

$$x_j \frac{dx}{dt} = \int_0^{t_j} v(p, t)^2 dt \quad (9)$$

Assume that the velocity between successive events is a constant v_{interval} , and subtract (9) with $j+1$ from (9) with j to get

$$(x_{j+1} - x_j) \frac{dx}{dt} = (t_{j+1} - t_j) v_{\text{interval}}^2 \quad (10)$$

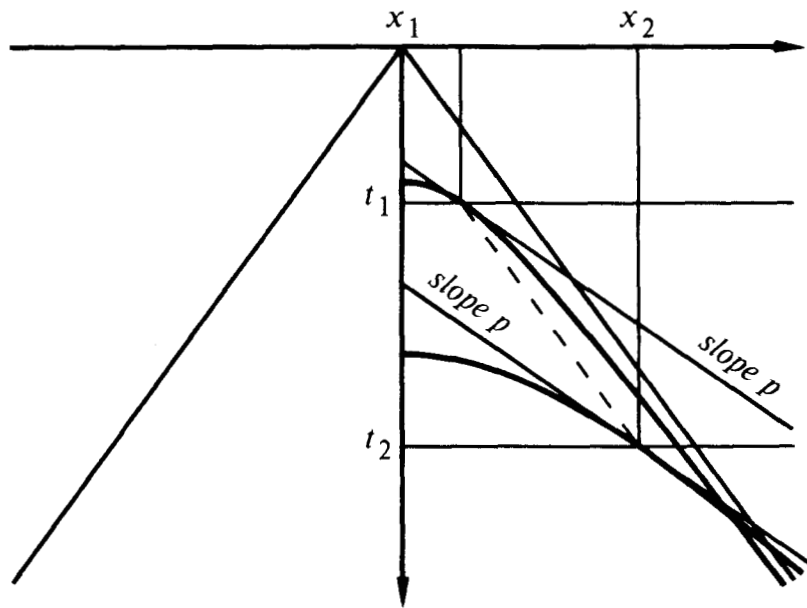


FIG. 5.4-2. Construction of two parallel lines on a common-midpoint gather which are tangent to reflections from two plane layers. (Gonzalez)

Solving for the interval velocity gives

$$v_{\text{interval}}^2 = \frac{x_{j+1} - x_j}{t_{j+1} - t_j} \frac{dx}{dt} \quad (11)$$

So the velocity of the material between the j^{th} and the $j+1^{\text{st}}$ reflectors can be measured directly using the square root of the product of the two slopes in (11), which are the dashed and solid straight lines in figure 2. The advantage of manually placing straight lines on the data, over automated analysis, is that you can graphically visualize the noise sensitivity of the measurement, and you can select on the data the best offsets at which to make the measurement.

If you do this routinely you quickly discover that the major part of the effort is in accurately constructing two lines that are tangent to the events. When you run into difficulty, you will find it convenient to replot the data with linear moveout $t' = t - px$. After replotting, the lines are no longer sloped but horizontal, so that any of the many timing lines can be used. Locating tangencies is now a question of finding the tops of convex events. This is shown in figure 3.

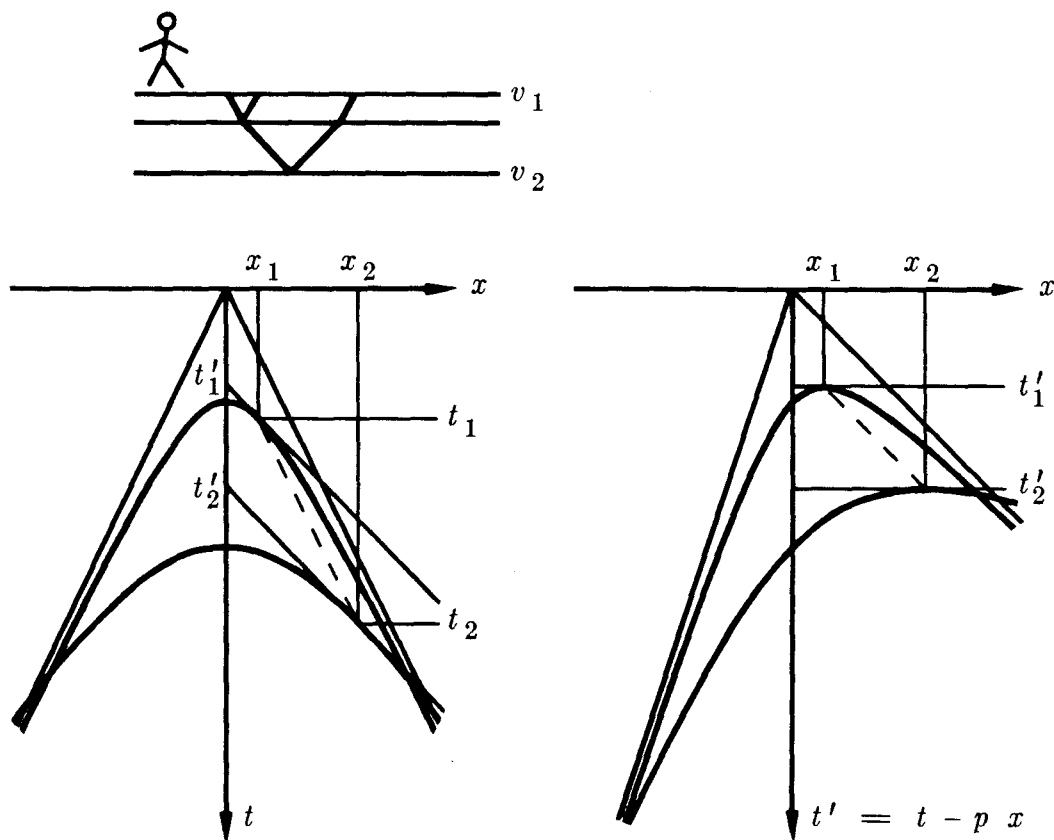


FIG. 5.4-3. Measurement of interval velocity by linear moveout. (Gonzalez)

In terms of the time t' , equation (11) is

$$v_{\text{interval}}^2 = \frac{1}{\frac{\Delta t}{\Delta x}} \frac{1}{p} = \frac{1}{\frac{\Delta t'}{\Delta x} + p} \frac{1}{p} \quad (12)$$

Earth velocity is measured on the right side of figure 3 by measuring the slope of the dashed line, namely $\Delta t'/\Delta x$, and inserting it into equation (12). (The value of p is already known by the amount of linear moveout that was used to make the plot).

Common-Midpoint Snell Coordinates

Common-*midpoint* slanted wave analysis is a more conservative approach to seismic data analysis than the Snell wave approach. The advantage of common-midpoint analysis is that the effects of earth dip tend to show up mainly on the midpoint axis, and the effect of seismic velocity shows up mainly on the offset axis. Our immediate goal is to define an invertible, wave-equation approach to determination of interval velocity.

The disadvantage of common-midpoint analysis is that it is nonphysical. A slant stack at common geophone simulates a downgoing Snell wave, and you expect to be able to write a differential equation to describe it, no matter what ensues, be it multiple reflection or lateral velocity variation. A common-*midpoint* slant stack does not model anything that is physically realizable. Nothing says that a partial differential equation exists to extrapolate such a stack. This doesn't mean that there is necessarily anything wrong with a common-midpoint *coordinate* system. But it does make us respect the Snell wave approach even though its use in the industrial world is not exactly growing by leaps and bounds.

(Someone implementing common-midpoint slant stack would immediately notice that it is easier than slant stack on common-geophone data. This is because at a common midpoint, the tops of hyperboloids must be at zero offset, the location of the Fresnel zone is more predictable, and interpolation and missing data problems are much alleviated).

Seismic data is collected in time, geophone, shot, and depth coordinates (t, g, s, z) . A new four-component system will now be defined. Midpoint is defined in the usual way:

$$y(t, g, s, z) = \frac{g + s}{2} \quad (13)$$

Travel-time depth is defined using the vertical phase velocity in a borehole. Two-way travel times are used, in order to be as conventional as possible:

$$\pi(t, g, s, z) = 2z \frac{\cos \theta}{v} \quad (14)$$

Next the surface offset h' is defined. We will not use the old definition of offset. For this method, shots and geophones should not go straight down, but along a ray. This can be so if h' is defined as follows:

$$h'(t, g, s, z) = \frac{g - s}{2} + z \tan \theta \quad (15)$$

With this new definition of h' the separation of the shot and geophone decreases with depth for constant h' .

Define the *LMO time* as the travel time in the point-source experiment less the linear moveout. So, at any depth, the LMO time is $t - p(g - s)$. As h' was defined to be the *surface* half-offset, t' is defined to be the *surface* LMO time. From the LMO time of a buried experiment, the LMO time at the surface is defined by adding in the travel-time depth of the experiment:

$$t' = t - p(g - s) + \tau \quad (16)$$

You may like to think of (16) as a “slant” on time retardation for upcoming waves, say, $t' = t_{LMO} + z_{slant}/v$. Formally,

$$t'(t, g, s, z) = t - p(g - s) + 2z \frac{\cos \theta}{v} \quad (17)$$

Figure 4 is a geometrical representation of these concepts.

From the geometry of figure 4 it will be deduced that a measurement of a reflection at some particular value of (h', t') directly determines the velocity. Write an equation for the reflector depth:

$$v \left(\frac{t'}{2} + p h' \right) \cos \theta = \text{reflector depth} = \frac{h'}{\tan \theta} \quad (18)$$

Using Snell’s law to eliminate angles and solving for velocity gives

$$v^2 = \frac{1}{p} \frac{1}{p + \frac{t'}{2h'}} \quad (19)$$

This is consistent with equation (12).

Gathering the above definitions into a group, and allowing for depth-

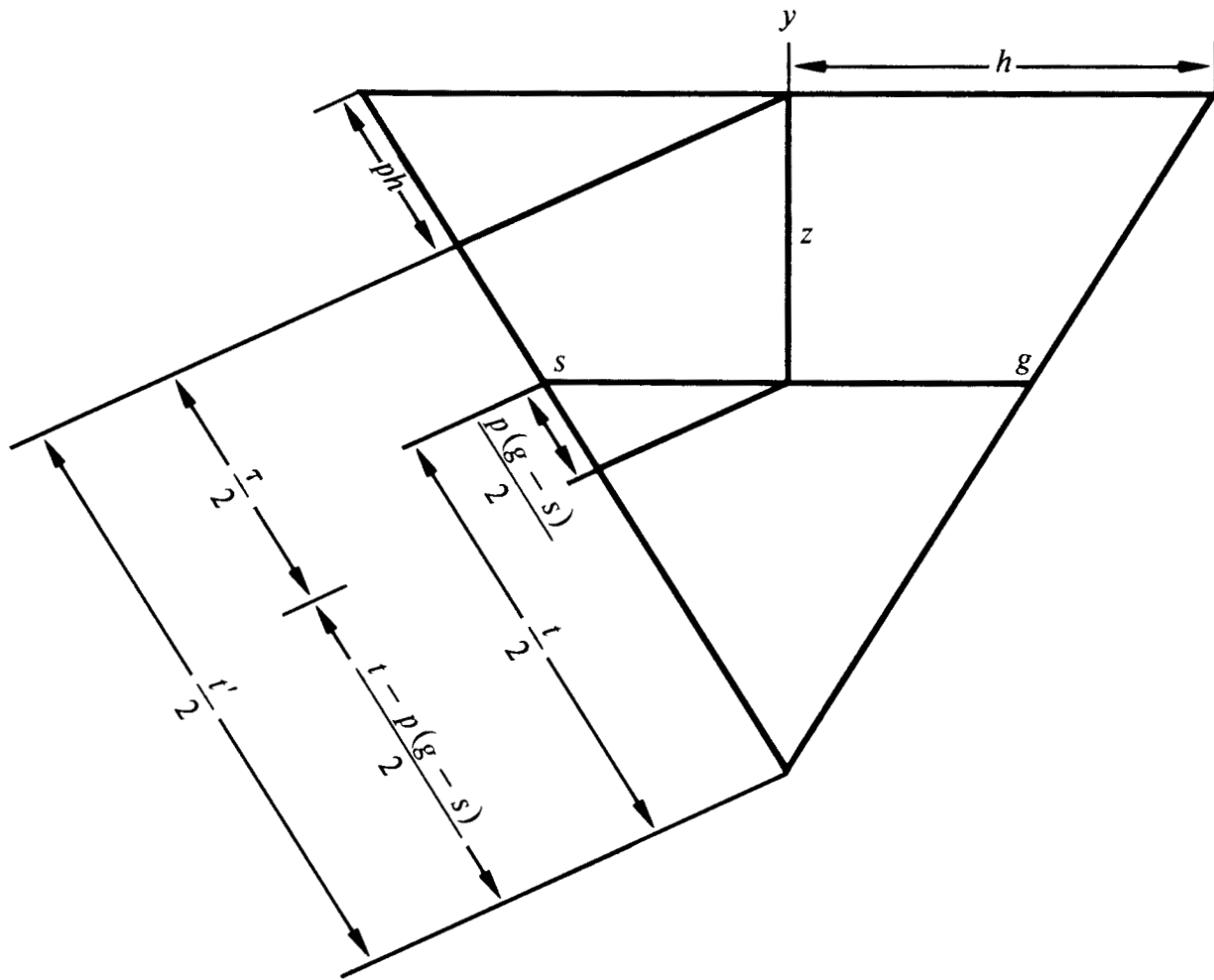


FIG. 5.4-4. The CMP-LMO coordinate frame geometry. This is a natural coordinate system for describing waves that resemble a reference Snell wave.

variable velocity by replacing z by the integral over z , we get

$$t'(t, g, s, z) = t - p(g - s) + 2 \int_0^z \frac{\cos \theta}{v} dz \quad (20a)$$

$$y(t, g, s, z) = \frac{g + s}{2} \quad (20b)$$

$$h'(t, g, s, z) = \frac{g - s}{2} + \int_0^z \tan \theta dz \quad (20c)$$

$$\tau(t, g, s, z) = 2 \int_0^z \frac{\cos \theta}{v} dz \quad (20d)$$

Before these equations are used, all the trigonometric functions must be eliminated by Snell's law for stratified media, $\sin \theta(z) = p v(z)$. Snell's parameter p is a numerical constant throughout the analysis.

The equation for interval velocity determination (12) again arises when dt'/dz from (20a) and dh'/dz from (20c) are combined:

$$\frac{dt'}{dh'} = \frac{2 \cos \theta}{v \tan \theta} \quad (21)$$

Eliminating the trig functions with $p v = \sin \theta$ allows us to solve for the interval velocity:

$$v^2 = \frac{1}{p} \frac{1}{p + \frac{1}{2} \frac{dt'}{dh'}} \quad (22)$$

At the earth's surface $z = 0$, seismic survey data can be put into the coordinate frame (20) merely by making a numerical choice of p and doing the linear moveout. No knowledge of velocity $v(z)$ is required so far. Then we look at the data for some tops of the skewed hyperbolas. Finding some, we use equation (12), (19) or (22) to get a velocity with which to begin downward continuation.

Waves can be described in either the (t, g, s, z) physical coordinates or the newly defined coordinates (t', y, h', τ) . In physical coordinates the image is found at

$$t = 0 \quad \text{and} \quad g = s \quad (23a,b)$$

To express these conditions in the Snell coordinates, insert (23) into (20a) and (20d). The result is what programmers call the stopping condition:

$$t' = \tau \quad (24)$$

This is the depth at which the velocity information should be best focused in the (h', t') -plane. Next some downward-continuation equations.

Differential Equations and Fourier Transforms

The chain rule for partial differentiation gives

$$\begin{bmatrix} \partial_t \\ \partial_g \\ \partial_s \\ \partial_z \end{bmatrix} = \begin{bmatrix} t'_t & y_t & h'_t & \tau_t \\ t'_g & y_g & h'_g & \tau_g \\ t'_s & y_s & h'_s & \tau_s \\ t'_z & y_z & h'_z & \tau_z \end{bmatrix} \begin{bmatrix} \partial_{t'} \\ \partial_y \\ \partial_{h'} \\ \partial_\tau \end{bmatrix} \quad (25)$$

In our usual notation the Fourier representation of the time derivative ∂_t is $-i\omega$. Likewise, ∂_t' , and the spatial derivatives $(\partial_y, \partial_{h'}, \partial_r, \partial_g, \partial_s, \partial_z)$ are associated with $i(k_y, k_{h'}, k_r, k_g, k_s, k_z)$. Using these Fourier variables in the vectors of (25) and differentiating (20) to find the indicated elements in the matrix of (25), we get

$$\begin{bmatrix} -\omega \\ k_g \\ k_s \\ k_z \end{bmatrix} = \begin{bmatrix} 1 & 0 & 0 & 0 \\ -p & 1/2 & 1/2 & 0 \\ p & 1/2 & -1/2 & 0 \\ \frac{2 \cos \theta}{v} & 0 & \tan \theta & \frac{2 \cos \theta}{v} \end{bmatrix} \begin{bmatrix} -\omega' \\ k_y \\ k_{h'} \\ k_r \end{bmatrix} \quad (26a,b,c,d)$$

Let S be the sine of the takeoff angle at the source and let G be the sine of the emergent angle at the geophone. If the velocity v is known, then these angles will be directly measurable as stepouts on common-geophone gathers and common-shot gathers. Likewise, on a constant-offset section or a slant stack, observed stepouts relate to an apparent dip Y , and on a linearly moved-out common-midpoint gather, stepouts measure the apparent stepout H' . The precise definitions are

$$S = \frac{v k_s}{\omega} \quad G = \frac{v k_g}{\omega} \quad (27a,b)$$

$$Y = \frac{v k_y}{2\omega} \quad H' = \frac{v k_{h'}}{2\omega} \quad (27c,d)$$

With these definitions (26b) and (26c) become

$$G = p v + Y + H' = Y + (H' + p v) \quad (28a)$$

$$S = -p v + Y - H' = Y - (H' + p v) \quad (28b)$$

The familiar offset stepout angle H is related to the LMO residual stepout angle H' by $H' = H - p v$. Setting H' equal to zero means setting $k_{h'}$ equal to zero, thereby indicating integration over h' , which in turn indicates slant stacking data with slant angle p . Small values of H'/v or $k_{h'}/\omega$ refer to stepouts near to p .

Processing Possibilities

The double-square-root equation is

$$\frac{k_z}{\omega} = -\frac{1}{v} \left(\sqrt{1 - S^2} + \sqrt{1 - G^2} \right) \quad (29)$$

With substitutions (26a,d), and (27a,b) the DSR equation becomes

$$\frac{k_\tau}{\omega} = 1 - \frac{pv}{1 - p^2 v^2} H' - \frac{1}{2} \left\{ \left[1 - \frac{2pv(H' - Y) + (H' - Y)^2}{1 - p^2 v^2} \right]^{1/2} + \left[1 - \frac{2pv(H' + Y) + (H' + Y)^2}{1 - p^2 v^2} \right]^{1/2} \right\} \quad (30)$$

Equation (30) is an exact representation of the double-square-root equation in what is called *retarded Snell midpoint coordinates*.

The coordinate system (20) can describe any wavefield in any medium. Equation (20) is particularly advantageous, however, only in stratified media of velocity near $v(z)$ for rays that are roughly parallel to any ray with the chosen Snell parameter p . There is little reason to use these coordinates unless they "fit" the wave being studied. Waves that fit are those that are near the chosen p value. This means that H' doesn't get too big. A variety of simplifying expansions of (30) are possible. There are many permutations of magnitude inequalities among the three ingredients pv , H' , and Y . You will choose the expansion according to the circumstances. The appropriate expansions and production considerations, however, have not yet been fully delineated. But let us take a look at two possibilities.

First, any dataset can be decomposed by stepout into many datasets, each with a narrow bandwidth in stepout space — CMP slant stacks, for example. For any of these datasets, H' could be ignored altogether. Then (30) would reduce to

$$\frac{k_\tau}{\omega} = 1 - \frac{1}{2} \left\{ \left(1 - \frac{-2pvY + Y^2}{1 - p^2 v^2} \right)^{1/2} + \left(1 - \frac{+2pvY + Y^2}{1 - p^2 v^2} \right)^{1/2} \right\} \quad (31a)$$

or

$$\frac{k_\tau}{\omega} = 1 - \frac{1}{2 \sqrt{1 - p^2 v^2}} \left[\sqrt{1 - (Y - pv)^2} + \sqrt{1 - (Y + pv)^2} \right] \quad (31b)$$

The above approach is similar to the one employed by Richard Ottolini in his dissertation.

Next, let us make up an approximation to (30) which is separable in Y and H' . We will be using separation methodology introduced in Section 3.4. Equation (31b) provides the first part. Then take $Y = 0$ and keep *all* terms up to quadratics in H' :

$$\frac{k_\tau}{\omega} = \frac{H'^2}{2(1 - p^2 v^2)^2} \quad (32)$$

A separable approximation of (30) is (31b) plus (32). It is no accident that there are no linear powers of H' in (32). The coordinate system was designed so that energy near the chosen model $Y = 0$ and $H = pv$ should not drift in the (h', t') -plane as the downward continuation proceeds.

The velocity spectrum idea represented by equation (32) is to use the H' term to focus the data on the (h', t') -plane. After focusing, it should be possible to read interval velocities directly as slopes connecting events on the gathers. This approach was used in the dissertation of Alfonso Gonzalez [1982].

EXERCISE

1. A hyperbola is identified on a zero-offset section. The top is obscured but you can measure (p, x, t) at two places. What is the earth velocity? Given the same measurements on a field profile (constant s) what is the earth velocity?

5.5 Multiple Reflection, Current Practice

Near the earth's surface are a variety of unconsolidated materials such as water, soil, and the so-called weathered zone. The contrast between these near-surface materials and the petroleum reservoir rocks below is often severe enough to produce a bewildering variety of near-surface resonances. These resonance phenomena are not predicted and cannot be explained by the methods described in previous chapters.

Hard Sea Floor Example

Figure 1 shows textbook-quality multiple reflections from the sea floor. Hyperbolas $v^2 t^2 - x^2 = z_j^2$ appear at uniform intervals $z_j = j \Delta Z$, $j = 0, 1, 2, \dots$. The data is unprocessed other than by multiplication by a spherical divergence correction t . Air is slower and lighter than water while sea-floor sediment is almost always faster and denser. This means that

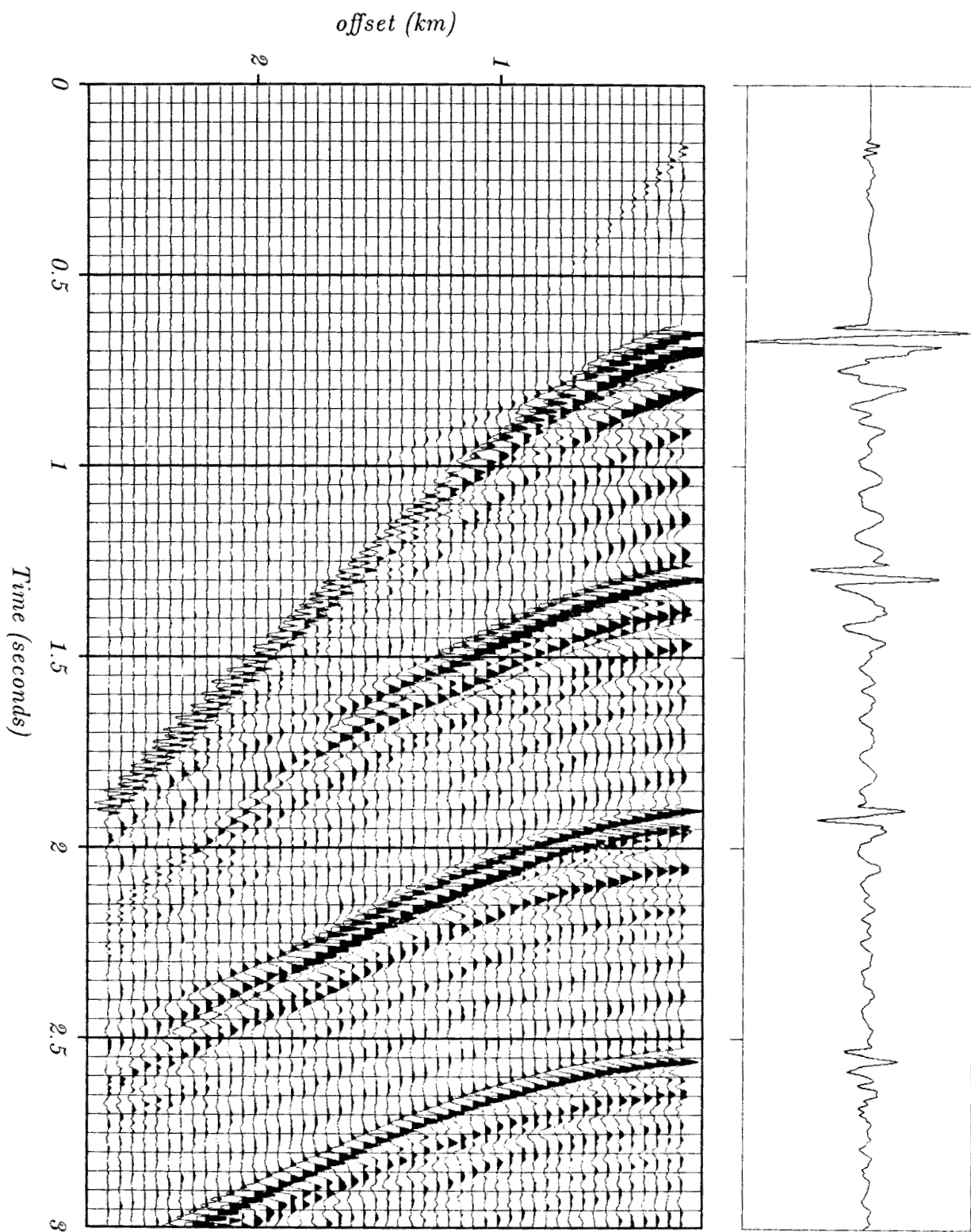


FIG. 5.5-1. Marine profile of multiple reflections from Norway. At the right, the near trace is expanded. (GECO)

successive multiple reflections almost always have alternating polarity. The polarity of a seismic arrival is usually ambiguous, but here the waveform is distinctive and it clearly alternates in polarity from bounce to bounce. The ratio of amplitudes of successive multiple reflections is the reflection coefficient. In figure 1, the reflection coefficient seems to be about -0.7 . Multiply reflected head waves are also apparent, as are alternating polarities on them. Since the head-wave multiple reflections occur at critical angle, they should have a -1.0 reflection coefficient. We see them actually increasing from bounce to bounce. The reason for the increase is that the spherical-divergence correction is based on three-dimensional propagation, while the head waves are really spreading out in two dimensions.

Multiple reflections are fun for wave theorists, but they are a serious impediment to geophysicists who would like to see the information-bearing primary reflections that they mask.

Deconvolution in Routine Data Processing

The water depth in figure 1 is deeper than typical of petroleum prospecting. Figures 2 and 3 are more typical. In figure 2, the depth is so shallow it is impossible to discern bounces. With land data the base of the weathered zone is usually so shallow and indistinct that it is generally impossible to discern individual reflections. The word *shallow* as applied to multiple reflections is *defined* to mean that the reflections reoccur with such rapidity that they are not obviously distinguished from one another.

Statisticians have produced a rich literature on the subject of deconvolution. For them the problem is really one of estimating a source waveform, not of removing multiple reflections. There is a certain mathematical limit in which the multiple-reflection problem becomes equivalent to the source-waveform problem. This limit holds when the reverberation is confined to a small physical volume surrounding the shot or the geophone, such as the soil layer. The reason that the source-waveform and multiple-reflection problems are equivalent in this limit is that the downgoing wave from a shot is not simply intrinsic to the shot itself but also includes the local soil resonances. The word *ghost* in reflection seismology refers to the reflection of the source pulse from the surface (or sometimes from the base of the weathered layer). Because the source is so near to these reflectors, we often regard the ghost as part of the source waveform too.

An extensive literature exists on the vertical-incidence model of multiple reflections. Among wave-propagation theorists, the removal of all multiples is called *inversion*. It seems that for inversion theory to be applicable to the

real problem, the theory must include a way to deal with an unknown, spectrally incomplete, shot waveform.

Routine work today typically ignores inversion theory and presumes the mathematical limit within which multiples may be handled as a shot waveform. The basic method was first developed for the industry by Schneider, Larner, Burg, and Backus [1964] of GSI (figure 2). Despite many further theoretical developments and the continuing active interest of many practical workers, routine deconvolution is little changed.

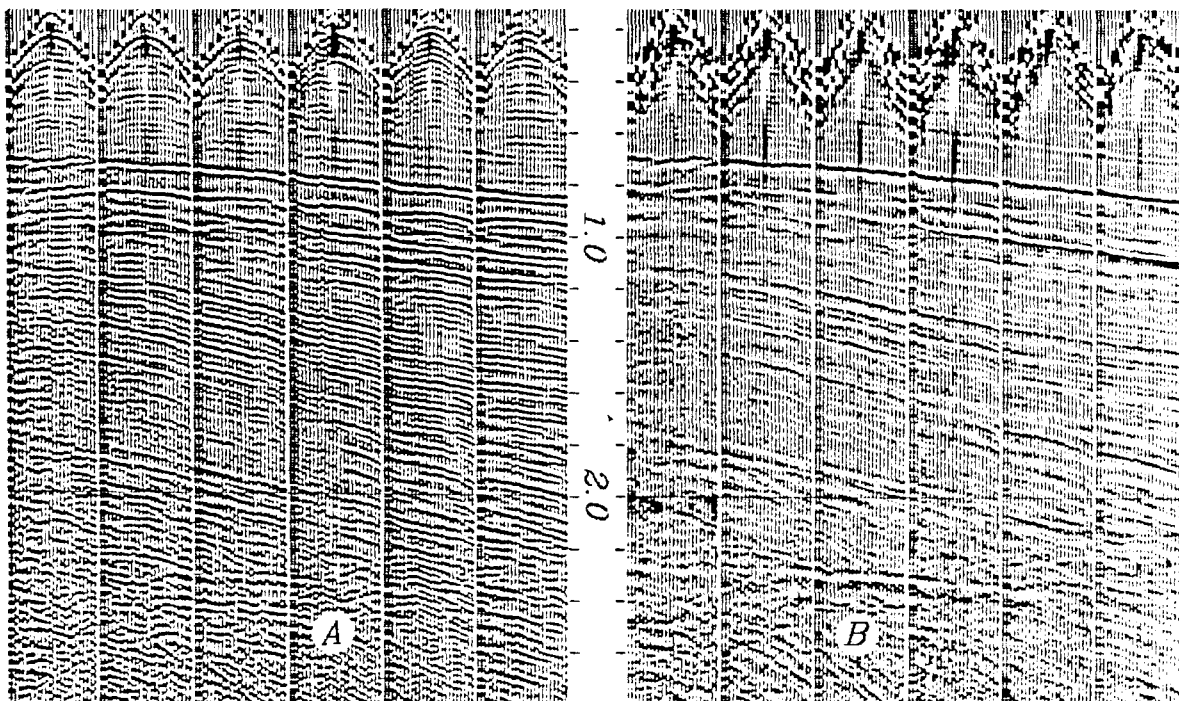


FIG. 5.5-2. Field profiles before (left) and after (right) deconvolution. (distributed by GSI, circa 1965)

Conventional industrial deconvolution (figure 2) has many derivations and interpretations. I will state in simple terms what I believe to be the essence of deconvolution. Every seismogram has a spectrum. The spectrum is a product of many causes. Some causes are of fundamental interest. Others are extraneous. It is annoying when a seismogram is resonant just because of some near-surface phenomena. Deconvolution is basically a process in which strong resonances are measured, and then a filter is designed to suppress them. The filter is designed to have a spectrum that is roughly inverse to the spectrum of the raw data. Thus the output of the filter is roughly white (equal amounts of all frequencies). From the earliest times,

seismologists have found that reflection seismic data rarely makes sense much outside the frequency band 10-100 Hz, so as a final step, frequencies outside the band are removed. (The assumption that the output spectrum should be white seems to most seismologists to be a weak assumption, but practice usually shows it better than interpreting earth images from raw data).

Another nonmathematical explanation of why deconvolution is a success in practice is that it equalizes the spectrum from trace to trace. It *balances* the spectra (Tufekcic et al [1981]). Not only is it annoying when a seismogram is resonant just because of some near-surface phenomena, but it is more annoying when the wave spectrum varies from trace to trace as the near surface varies from place to place. A variable spectrum makes it hard to measure stepouts. Notice that the conventional industrial deconvolution described above includes *spectral balancing* as a byproduct. Figure 3 shows data that needs spectral balancing.

The above interpretation of deconvolution and why it works is different from what is found in most of the geophysical literature. Deconvolution is often interpreted in terms of the predictability of multiple reflections and the nonpredictability of primary reflections. It is shown in FGDP how multiple reflections are predicted. They are predicted, not by a strictly convolutional model, but approximately so. Prediction by convolution works best when the reverberation is all in shallow layers. Then it is like a source waveform.

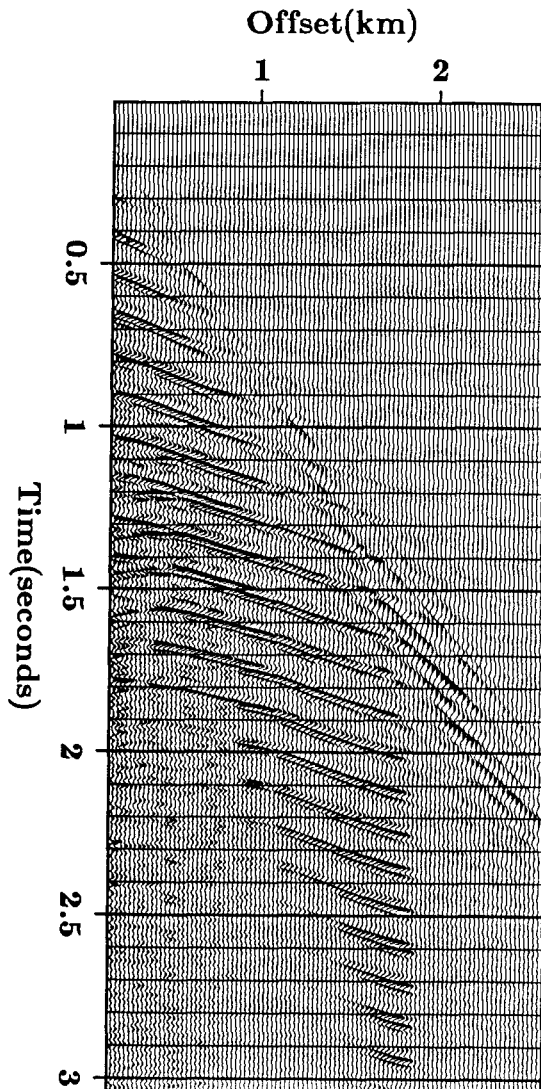
Cardiovascular research is well integrated with routine practice, whereas pulmonary research is not. I compare this to migration and velocity theory being a good guide to industrial practice, whereas deconvolution theory is less so. The larger gap between theory and practice is something to be aware of. Some fields are more resistant to direct attack. In them you progress by more indirect routes. This is confusing for the student and demoralizing for the impatient. But that is the way it is. For more details, see Ziolkowski [1984].

The next few pages show land data with buried geophones confirming that source waveforms are mainly near-surface reverberation. Then we turn to departures from the convolutional model.

A Vertical Seismic Profile (VSP)

Seismologists always welcome the additional information from a *vertical seismic profile* (VSP). A VSP is some collection of seismograms recorded from the surface to a borehole. Routine well-based measurements such as rock cuttings and electric logs record *local* information, often just centimeters from the well. It is nice to think of the earth as horizontal strata, but this idealization fails at some unknown distance from the well. Surface reflection

FIG. 5.5-3. Profile from the North Sea. (Western Geophysical) Observe strong reverberations with a period of about 90 ms. These are multiple reflections from the sea floor. Note that the strongest signal occurs at increasing offset with increasing time. This is because the strongest multiples are often at critical angle. The strength of the reverberation diminishes abruptly 1.8 km behind the ship. This implies that the sea floor changes abruptly at that point.



seismology, although it is further from the “ground truth” of well-bore measurements, provides the needed information about lateral continuity. But surface reflection data has resolving-power limitations as well as other uncertainties. The VSP provides information at an intermediate scale and also provides a calibration of the surface seismic method. Unfortunately, VSPs are costly and we rarely have them.

The subject of VSP occupies several books and many research papers. (See Gal'perin [1974] and Balch et al [1982]). Here we will just look at a single VSP to get some idea of source waveforms and multiple reflections. The VSP shown in figure 4 is from a typical land area. The multiple reflections are not so severe as with the marine data shown elsewhere in this chapter. The earliest arrival in figure 4 is the primary downgoing wave. Downgoing waves increase their travel time with depth, the slope of the arrival curve giving the downward component of velocity. After the first downgoing waves

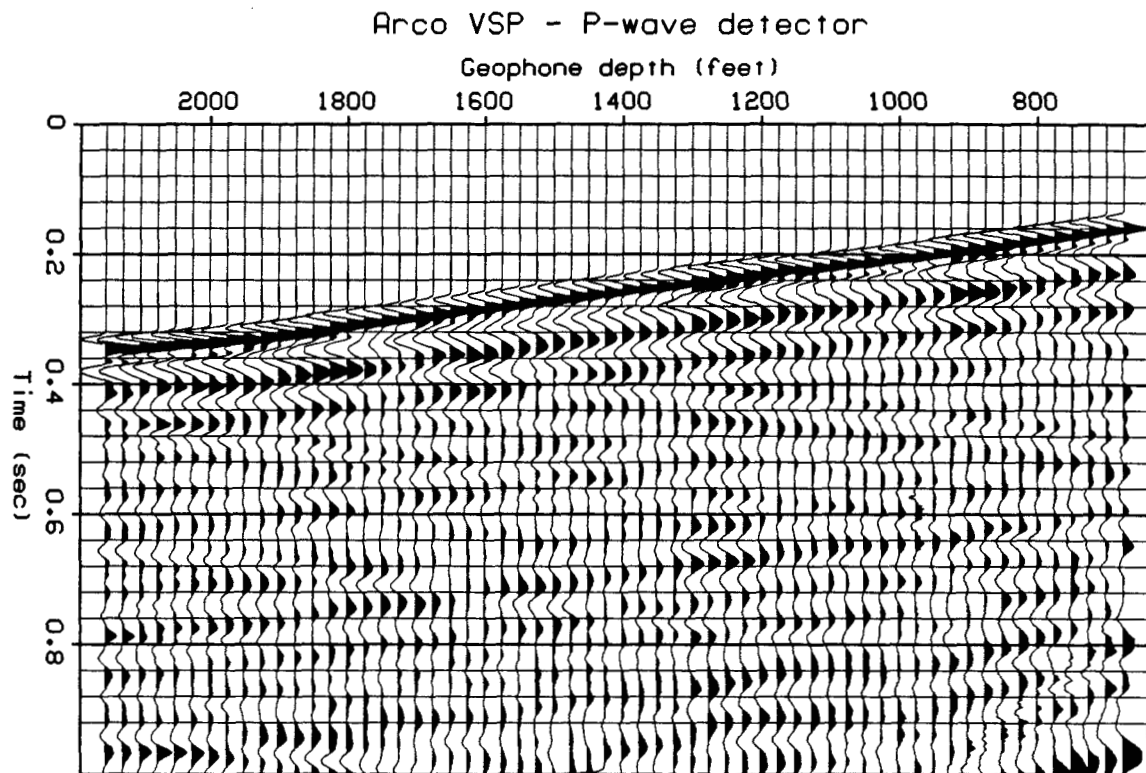


FIG. 5.5-4. Vertical seismic profile. The source is at the earth's surface near the borehole. The horizontal axis is the receiver depth. The vertical axis is travel time from zero to one second. Amplitudes are scaled by $t^{1.5}$. (ARCO)

arrive, you can see more downgoing waves with the same velocity. Upgoing waves have the opposite slope of the downgoing waves. These are also visible in figure 4.

Since late echoes are weaker than early ones, seismic data is normally scaled upwards with time before being displayed. There is no universal agreement in either theory or practice of what scaling is best. I have usually found t^2 scaling to be satisfactory for reflection data. (See Section 4.1). Figure 4 shows that $t^{1.5}$ scaling keeps the first arrival at about a constant amplitude on the VSP.

Viewing figure 4 from the side shows that the downgoing pulse is followed by a waveform that is somewhat consistent from depth to depth. The degree of consistency is not easy to see because of interference with the upcoming wave. As far as I can tell from the figure, the downgoing wave at the greatest depth is equal to that at the shallowest depth.

Figure 5 shows the same data augmented by some shallow receivers. You will notice that the downgoing wave no longer seems to be independent of

depth. So we can conclude that, as a practical matter, the downgoing waveform seems to be mainly a result of near-surface reverberation.

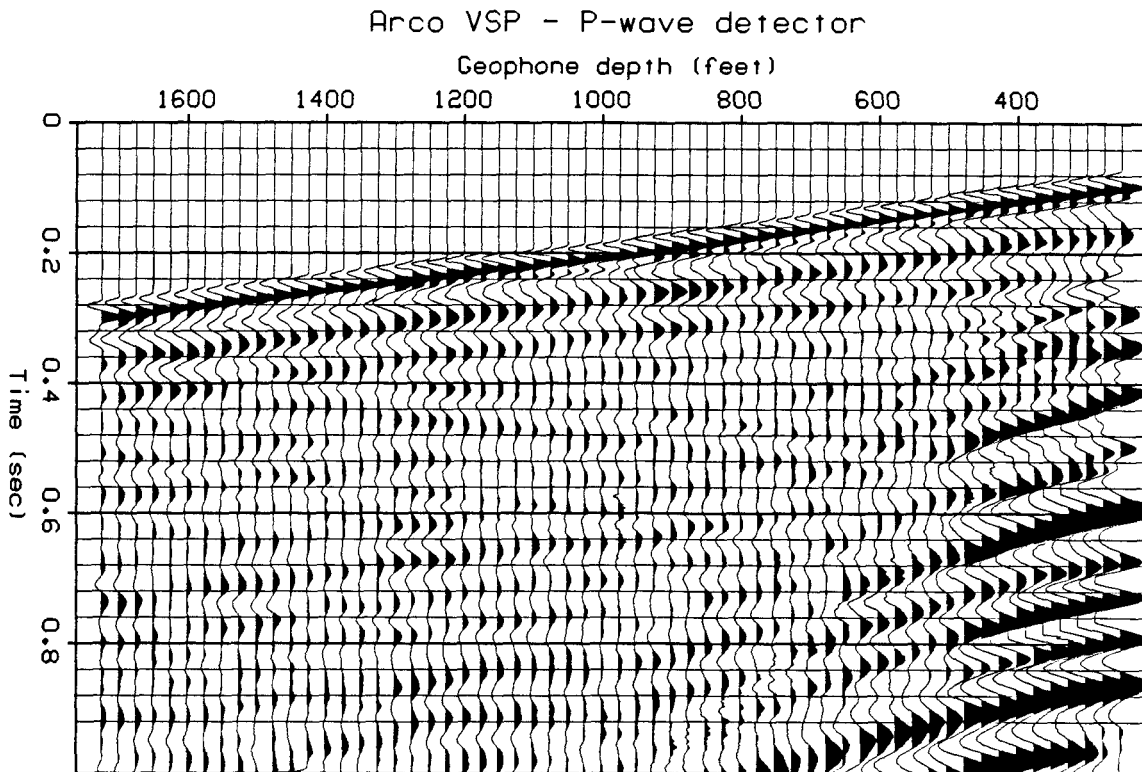


FIG. 5.5-5. The data of figure 4 augmented with shallower receivers. Amplitudes are scaled by $t^{1.5}$. (ARCO)

The energy in the first burst in figure 4 is roughly comparable to the remaining energy. The remaining energy would be less if the VSP were displayed without $t^{1.5}$ scaling, but since the surface reflection data is normally displayed with some such scaling (often t^2), it makes more sense statistically to speak of the energy on the scaled data. So the reverberating energy is roughly comparable to the first arriving energy.

Below the near-surface region, the downgoing wave changes slowly with depth. Now we should ask how much the downgoing wave would change if the experiment were moved laterally. Obviously the borehole will not move laterally and we will be limited to data where only the surface source moves laterally. Since near-surface variations often change rapidly in the lateral direction, we may fear that the downgoing waveform also changes rapidly with shot location. The reverberation near a shot is repeated similarly near

any surface receiver. The resulting composite reverberation is the convolution of near-shot reverberation and near-geophone reverberation. So to get the information needed to deconvolve surface seismic data, the VSP should be recorded with many surface source locations.

Unfortunately such *offset VSP* data is rarely available. When petroleum production declines and expensive secondary recovery methods are contemplated, the cost of VSP will not seem so high. The production lost during VSP acquisition may be more easily weighed against future gains.

Again we should think about the meaning of "bad" data. Seismic data is generally repeatable whenever it is above the level of the ambient microseismic noise. But often the signals make no sense. The spatial correlations mean nothing to us. Most data at late times fits this description. Perhaps what is happening is this: (1) The downgoing waveform is getting a long trail; (2) the trail is a chaotic function of the surface location; and (3) the energy in the trail exceeds the energy in the first pulse. So, with so much randomness in the downgoing wave, the upcoming wave is necessarily incomprehensible.

Deep Marine Multiples, a Phenomenon of Polar Latitudes

It has frequently been noted that sea-floor multiple reflection seems to be a problem largely in the polar latitudes only — rarely in equatorial regions. This observation might be dismissed as being based on the statistics of small numbers, but two reasons can be given why the observation may be true. Each of these is of interest whether or not the statistics are adequate.

It happens that natural gas is soluble in water and raises the temperature of freezing, particularly at high pressure. Ice formed when natural gas is present is called *gas hydrate*. Thus there can be, under the liquid ocean, trapped in the sediments, solid gas hydrate. The gas hydrate stiffens the sediment and enhances multiple reflections.

A second reason for high multiple reflections at polar latitudes has to do with glacial erosion. Ordinarily ocean bottoms are places of slow deposition of fine-grained material. Such freshly deposited rocks are soft and generate weak multiple reflections. But in polar latitudes the scouring action of glaciers removes sediment. Where erosion is taking place the freshly exposed rock is stronger and stiffer than newly forming sediments. Thus, stronger sea-floor reflections.

Continents erode and deposit at all latitudes. However, one might speculate that on balance, continental shelves are created by deposition in low and middle latitudes, and then drift to high latitudes where they erode. While

highly speculative, this theory does provide an explanation for the association of multiple reflections with polar latitudes.

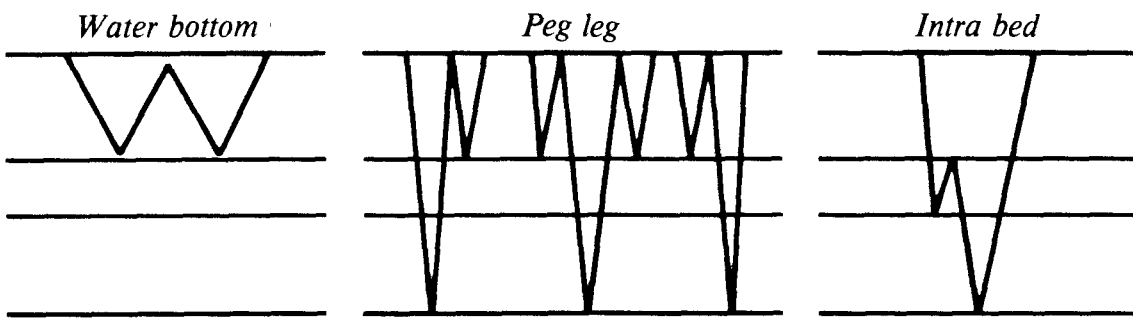


FIG. 5.5-6. Raypaths are displayed for (a) a water-bottom multiple, (b) a pegleg multiple family, and (c) a short-path multiple.

Pegleg and Intrabed Multiple Reflections

Multiple reflections fall into one of three basic categories — see figure 6.

Water-bottom multiples are those multiples whose raypaths lie entirely within the water layer (figure 6a). Since the sea floor usually has a higher reflectivity than deeper geological horizons, water-bottom multiples often have strong amplitudes. In deep water these multiples can be very clear and distinct. A textbook-quality example is shown in figure 1.

Pegleg multiple reflections are variously defined by different authors. Here pegleg multiples (figure 6b) are defined to be those multiples that undergo one reflection in the sedimentary sequence and other reflections in the near surface.

To facilitate interpretation of seismic data, let us review the timing and amplitude relations of vertical-incidence multiple reflections in layered media. Take the sea-floor two-way travel time to be t_1 with reflection coefficient c_1 . Then the n^{th} multiple reflection comes at time $n t_1$ with reflection strength c_1^n . Presume also a deeper primary reflection at travel-time depth t_2 with reflection coefficient c_2 . The sea-floor peglegs arrive at times $t_2 + n t_1$. Note that peglegs come in families. For example, the time $t_2 + 2t_1$ could arise from three paths, $t_2 + 2t_1$, $t_1 + t_2 + t_1$, or $2t_1 + t_2$. So the n^{th} order pegleg multiple echo is really a summation of $n + 1$ rays, and thus its strength is proportional to $(n + 1) c_2 c_1^n$. The sea-floor reverberation is c_1^n , which is not the same function of n as the function that describes reverberation on sediments, $(n + 1) c_1^n$. Ignoring the sea-floor

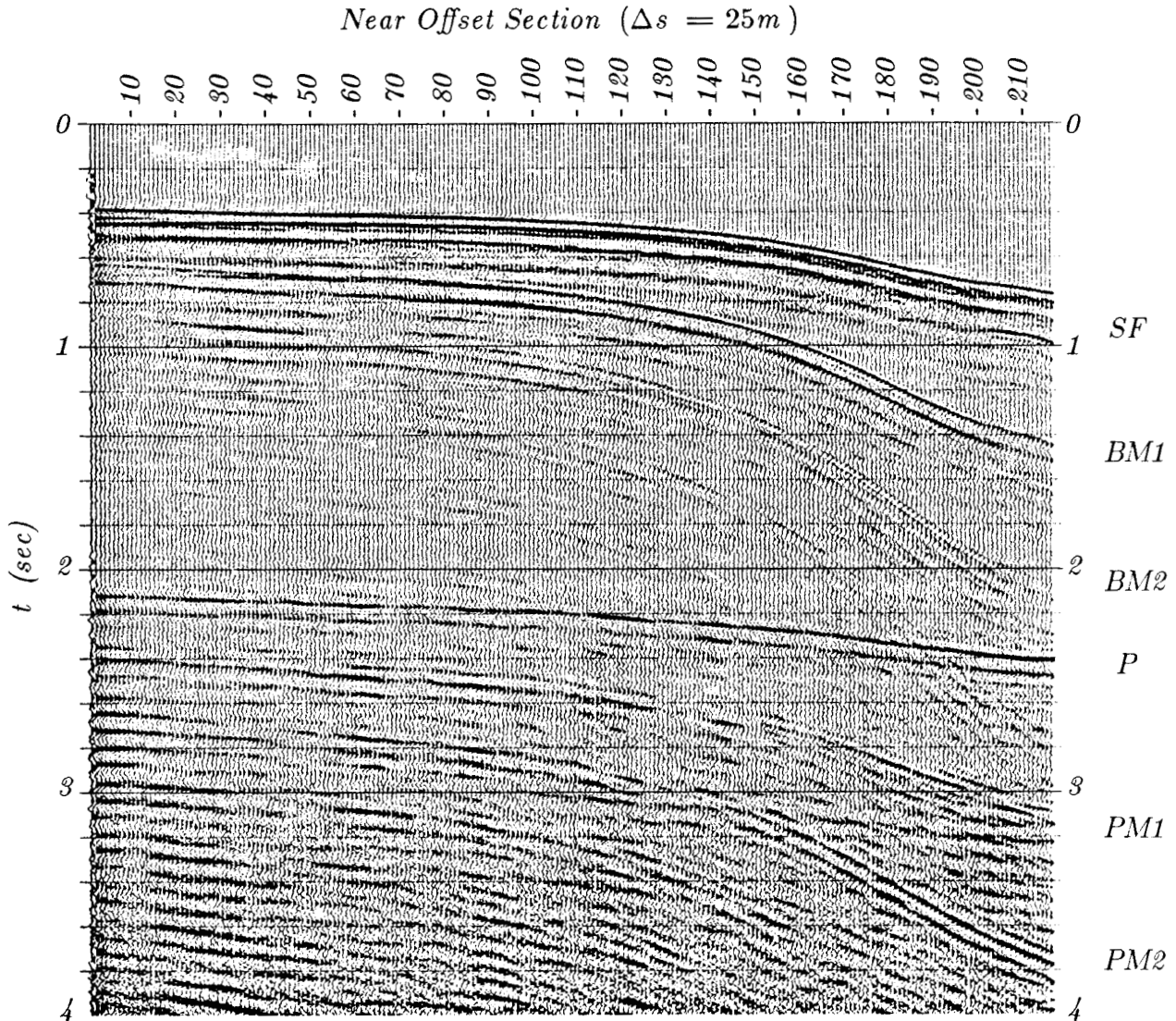


FIG. 5.5-7. Near-offset section — offshore Labrador (Flemish Cap). The offset distance is about 9 shotpoints. SF = sea floor, BM1 = first bottom multiple, BM2 = second bottom multiple, P = primary, PM1 = first pegleg multiple, and PM2 = second pegleg multiple. (AMOCO-Canada, Morley)

reverberation itself you can just think of $(n + 1) c_1^n$ as a shot waveform.

Every multiple must have a “turn-around” where an upcoming wave becomes a downgoing wave. Almost all readily recognized multiples are *surface* multiples, that is, they have their turn-arounds at the earth’s surface. Figure 7 shows some clear examples. In land data the turn-around can be at the base of the soil layer, which is almost the same as being at the earth’s surface.

A raypath that is representative of yet another class of multiples, called *short-path* or *intrabed* multiples, is shown in figure 6c. Their turn-around is *not* at or near the earth's surface. These multiples are rarely evident in field data, although figure 8 shows a clear case in which they are. When they are identified, it is often because the seismic data is being interpreted using some accompanying well logs. The reason that short-path multiples are so rarely observed compared to peglegs is that the reflection coefficients within the sedimentary sequence are so much lower than on the free surface. The weakness of individual short-path multiples may be compensated for, however, by the *very large* numbers in which they can occur. Any time a seismic section becomes incomprehensible, we can hypothesize that the data has become overwhelmed by short-path multiples.

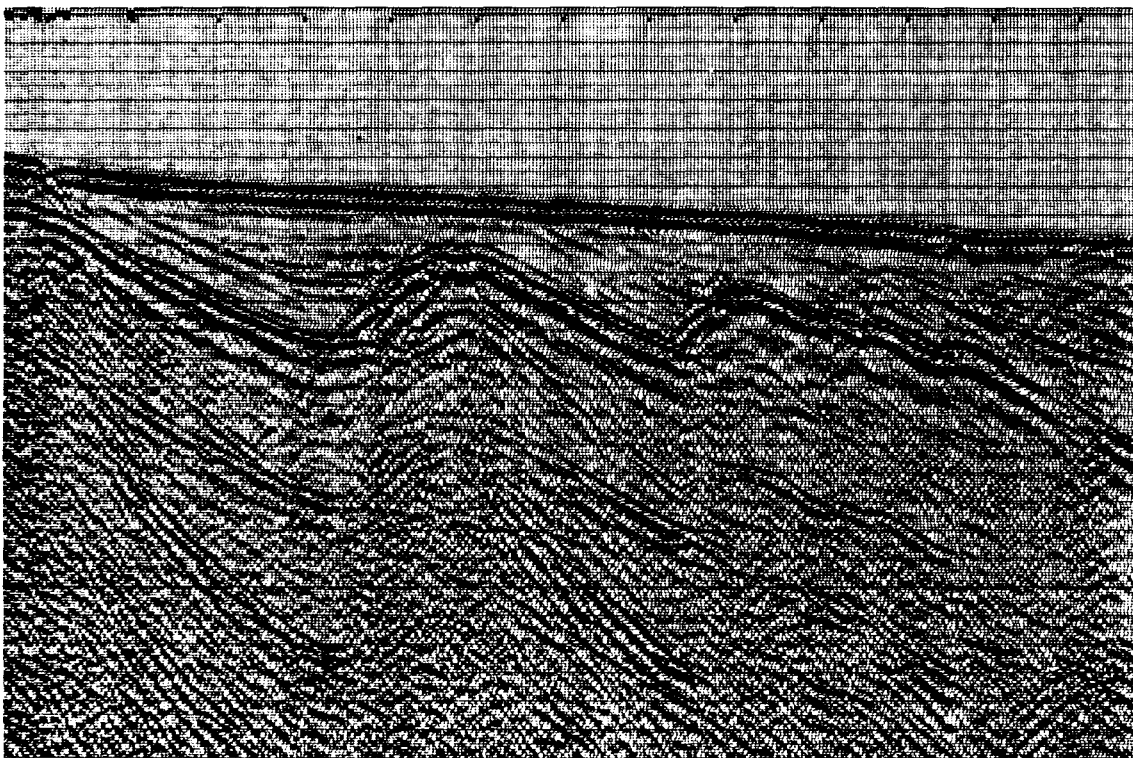


FIG. 5.5-8. A rare case of unambiguous intrabed multiple reflections. The data was recorded near Puerto Rico. The inner-bed multiple is between the sea floor and the basement. Thus its travel time is $t_{base} + (t_{base} - t_{floor})$. Do you see it? (Western Geophysical)

The Need to Distinguish between Types of Sections

By 1974, wave-equation methods had established themselves as a successful way to migrate CDP-stacked sections. Bolstered by this success, Don Riley and I set out to apply the wave equation to the problem of predictive suppression of deep-water multiple reflections. Hypothesizing that diffraction effects were the reason for all the difficulty that was being experienced then with deep-water multiple reflection, we developed a method for the modeling and predictive removal of diffracted multiple reflections (see FGDP, Chapter 11-4). We didn't realize that in practice the multiple reflection problem would be so much more difficult than the primary reflection problem. For primaries, the same basic migration method works on zero-offset sections, CDP-stacked sections, or vertical-incidence plane-wave sections. Our multiple-suppression method turned out to be applicable only to vertical plane-wave stacks. Don Riley prepared figure 9, which shows some comparisons.

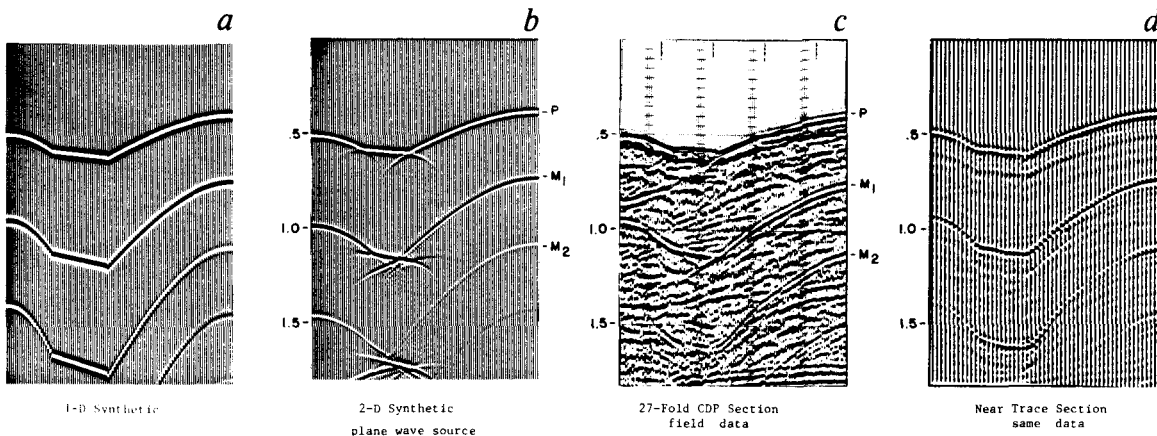


FIG. 5.5-9. Diffracted multiple-reflection examples: (a) 1-D synthetic, (b) 2-D synthetic, vertical plane-wave source, (c) 27-fold CDP data section (GSI), (d) near-trace section. (Riley)

One thing to keep in mind while studying the comparisons in figure 9 is that on the field data there are likely to be aspects of propagation in three dimensions that may go unrecognized. The third dimension is always a “skeleton in the closet.” It doesn’t usually spoil two-dimensional migration, but that doesn’t assure us that it won’t spoil 2-D wave-equation multiple suppression.

Examples of Shallow-Water Multiples with Focusing

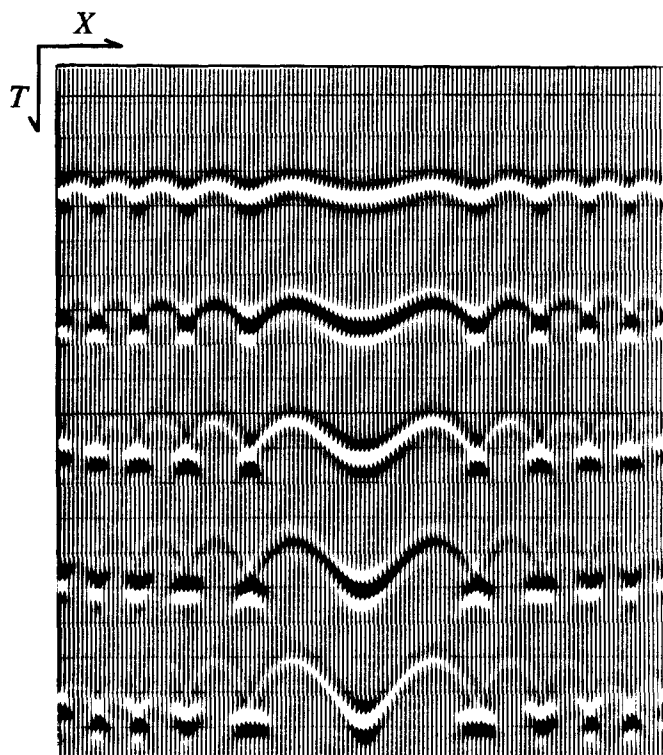
The exploding-reflector concept does not apply to multiple reflections, so there is no simple wave-theoretic means of predicting the focusing behavior of multiples on a near-trace section. Luckily multiples on vertical plane-wave stacks are analyzable. They may give us some idea about the focusing behavior of multiple reflections on other seismic sections. A vertically down-going plane wave is simulated by a common-geophone stack without moveout. This isn't the same as the familiar CDP stack, but it is analyzable with the techniques described in Chapters 1 and 2.

Consider a multiple reflection that has undergone several surface bounces. The seismic energy started out as a downgoing plane wave. It remained unchanged until its first reflection from the sea floor. The sea-floor bounce imposed the sea-floor topography onto the plane wave. In a computer simulation the topography would be impressed upon the plane wave by a step with the lens equation. Then the wave diffracted its way up to the surface and back down to the sea floor. In a computer another topographic lens shift would be applied. The process of alternating diffraction and lensing would be repeated as often as you would care to keep track of things. Figure 10 shows such a simulation. A striking feature of the high-order multiple reflections in figure 10 is the concentration of energy into localized regions. It is easy to see how bounces from concave portions of the sea floor can overcome the tendency of acoustic energy to spread out. These regions of highly concentrated energy that occur late on the time axis do not resemble primaries at all. With primaries a localized disturbance tends to be spread out into a broad hyperbola. Primary migration of the highly concentrated bursts of energy seen on figure 10 must lead to semicircles. Such semicircles are most unlikely geological models — and are all too often predicted by the industry's best migration programs.

The most important thing to learn from the synthetic multiple reflections of figure 10 is that multiples need not resemble primaries. Semicircles that occur on migrated stacks could be residual multiple reflections. Unfortunately, there is no simple theory that says whether or not focused multiples on vertical wave stacks should resemble those on zero-offset sections or CDP stacks. Luckily some data exists that provides an answer. Figure 11 is a zero-offset section which establishes that such focusing phenomena are indeed found in qualitative, if not quantitative, form on reflection survey data.

The marine data exhibited in figure 11 clearly displays the focusing phenomena in the synthetic calculations of figure 10. This suggests that we should utilize our understanding in a quantitative way to predict and suppress the multiple reflections in order to get a clearer picture of the earth's

FIG. 5.5-10. Simulated sea-floor multiple reflections. The vertical exaggeration is 5. Little focusing is evident on the gentle sea-floor topography, but much focusing is evident on high-order multiple reflections. At late times there is a lack of lateral continuity, really unlike primary reflection data.



subsurface. There are several reasons why this would not be easy to do. First, the Riley theory applies to vertical wave stacks. These are quantitatively different from common-midpoint stacks. Second, the effective seismic sea-floor depth is not a known input: it must somehow be determined from the data itself. Third, the water depth in figure 11 is so shallow that individual bounces cannot be distinguished.

Why Deconvolution Fails in Deep Water

It has been widely observed that deconvolution generally fails in deep water. A possible reason for this is that deep water is not the mathematical limit at which the multiple-reflection problem is equivalent to the shot-waveform problem. But that is not all. Theory predicts that under ordinary circumstances multiples should alternate in polarity. The examples of figure 1 and figure 2 confirm it. You will have trouble, however, if you look for alternating polarity on CDP stacks. The reason for the trouble also indicates why deconvolution tends to fail to remove deep multiples from CDP stacks.

Recall the timing relationships for multiples at zero offset. The *reverberation period* is a constant function of time. Because of moveout, this is not the case at any other offset. Normal-moveout correction will succeed in

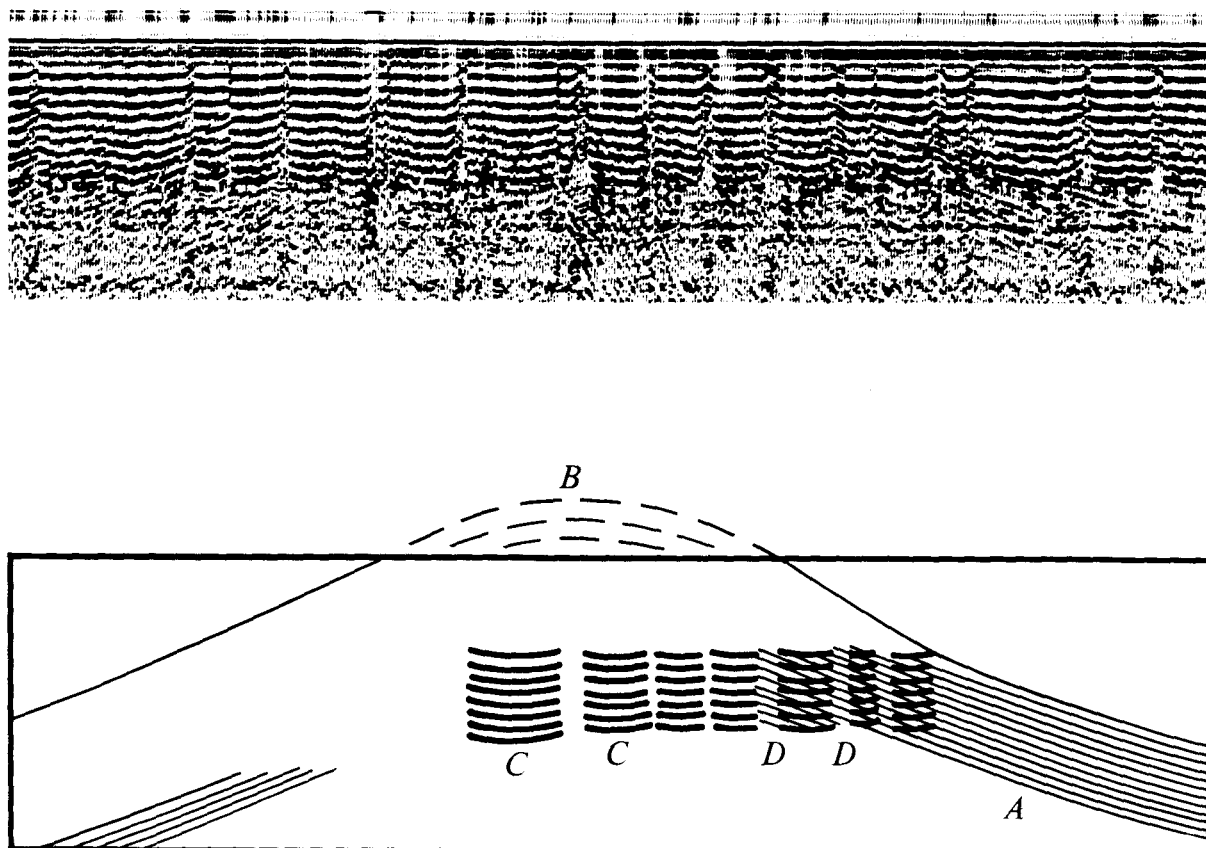


FIG. 5.5-11. Example of focusing effects on multiple reflections in near-trace section at Chukchi Sea. These effects are obscured by stacking. (U.S. Geological Survey)

- A. Existing structure.
- B. Former structure unevenly eroded away leaving localities of sea floor convex or concave.
- C. High order multiple reflections focusing where the sea floor is concave.
- D. Existing structural dip exposed in windows where the multiples are weak (i.e., where convex sea floor causes multiple to spread rapidly).

restoring zero-offset timing relationships in a constant-velocity earth, but when the velocity increases with depth, the multiples will have a slower RMS velocity than the primaries. So the question is what velocity to use, and whether, in typical land and marine survey situations, the residual time shifts are greater than a half-wavelength. No equations are needed to answer this question. All that is needed is the general observation that conventional common-midpoint stacking suppresses multiples because they have lower velocities than primaries. This observation implies that normal moveout routinely time shifts multiple reflections a half-wavelength or more out of their natural zero-offset relationships.

To make matters worse, the amplitude relationships that we expect at zero offset are messed up. Reflection coefficient is a function of angle. But on a seismogram from some particular offset, each multiple reflection will have reflected at a different angle.

Vertical incidence timing relationships are *approximately* displayed on CDP stacks. The practical difficulty is that the CDP stack does not mimic the vertical-incidence situation well enough to enable satisfactory prediction of multiples from primaries.

Before stack, on marine data, moveout could be done with water velocity, but then any peglegs would not fit the normal-incidence timing relationship. Since peglegs are often the worst part of the multiple-reflection problem, moveout should perhaps be done with pegleg velocity. No matter how you look at it, all the timing relationships for deep multiple reflections cannot be properly adjusted by moveout correction.

EXERCISE

1. On some land data it was noticed that a deep multiple reflection arrived a short time earlier than predicted by theory. What could be the explanation?

5.6 Multiple Reflection — Prospects

To improve our ability to suppress multiples, we try to better characterize them. The trouble is that a realistic model has many ingredients. Few of the theories that abound in the literature have had much influence on routine industrial practice. I would put these unsuccessful theories into two categories:

1. Those that try to achieve everything with statistics, oversimplifying the complexity of the spatial relations
2. Those that try to achieve everything with mathematical physics, oversimplifying the noisy and incomplete nature of the data

Multiple reflection is a good subject for nuclear physicists, astrophysicists, and mathematicians who enter our field. Those who are willing to take up the challenge of trying to carry theory through to industrial practice are rewarded by learning some humility. I'll caution you now that I haven't pulled it all together in this section either!

Here two approaches will be proposed, both of which attend to geometry *and* statistics. Both approaches are new and little tested. Regardless of how well they may work, I think you will find that they illuminate the task.

The first approach, called *CMP slant stack*, is a simple one. It transforms data into a form in which all offsets mimic the simple, one-dimensional, zero-offset model. The literature about that model in both statistics and mathematical physics is extensive.

The second approach is based on a *replacement impedance* concept. It is designed to accommodate rapid lateral variations in the near surface. It is easiest to explain for a hypothetical marine environment where the sole difficulty arises from lateral variation in the sea-floor reflectivity. The basic idea is downward continuation of directional shots and directional geophones to just beneath the sea floor, but no further. This is followed by upward continuation through a replacement medium that has a zero sea-floor reflection coefficient. This process won't eliminate all the multiple reflections, but it should eliminate the most troublesome ones.

Transformation to One Dimension by Slant Stack

A rich literature (c.f. FGDP) exists on the one-dimensional model of multiple reflections. Some authors develop many facets of wave-propagation theory. Others begin from a simplified propagation model and develop many facets of information theory. These one-dimensional theories are often regarded as applicable only at zero offset. However, we will see that all other offsets can be brought into the domain of one-dimensional theory by means of slant stacking.

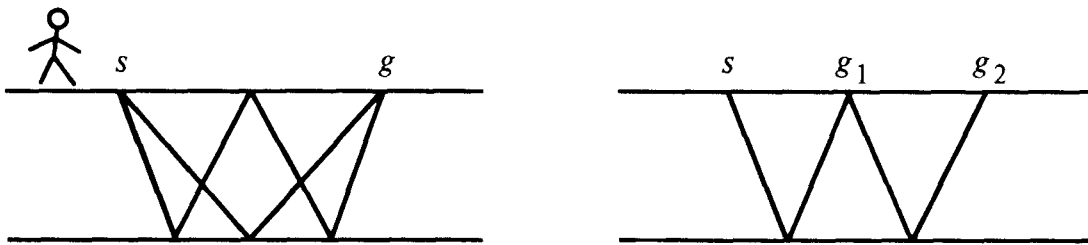


FIG. 5.6-1. Rays at constant-offset (left) arrive with various angles and hence various Snell parameters. Rays with constant Snell parameter (right) arrive with various offsets. At constant p all paths have identical travel times.

The way to get the timing and amplitudes of multiples to work out like vertical incidence is to stop thinking of seismograms as time functions at constant offset, and start thinking of constant Snell parameter. In a layered earth the complete raypath is constructed by summing the path in each layer. At vertical incidence $p = 0$, it is obvious that when a ray is in layer j its travel time t_j for that layer is independent of any other layers which may also be traversed on other legs of the total journey. This independence of travel time is also true for any other fixed p . But, as shown in figure 1, it is not true for a ray whose total offset $\sum f_j$, instead of its p , is fixed. Likewise, for fixed p , the horizontal distance f_j which a ray travels while in layer j is independent of other legs of the journey. Thus, in addition, $t_j + \text{const } f_j$ for any layer j is independent of other legs of the journey. So $t_j' = t_j - pf_j$ is a property of the j^{th} layer and has nothing to do with any other layers which may be in the total path. Given the layers that a ray crosses, you add up the t_j and the f_j for each layer, just as you would in the vertical-incidence case. Some paths are shown in figure 2.

To see how to relate field data to slant stacks, begin by searching on a common-midpoint gather for all those patches of energy (tangency zones)

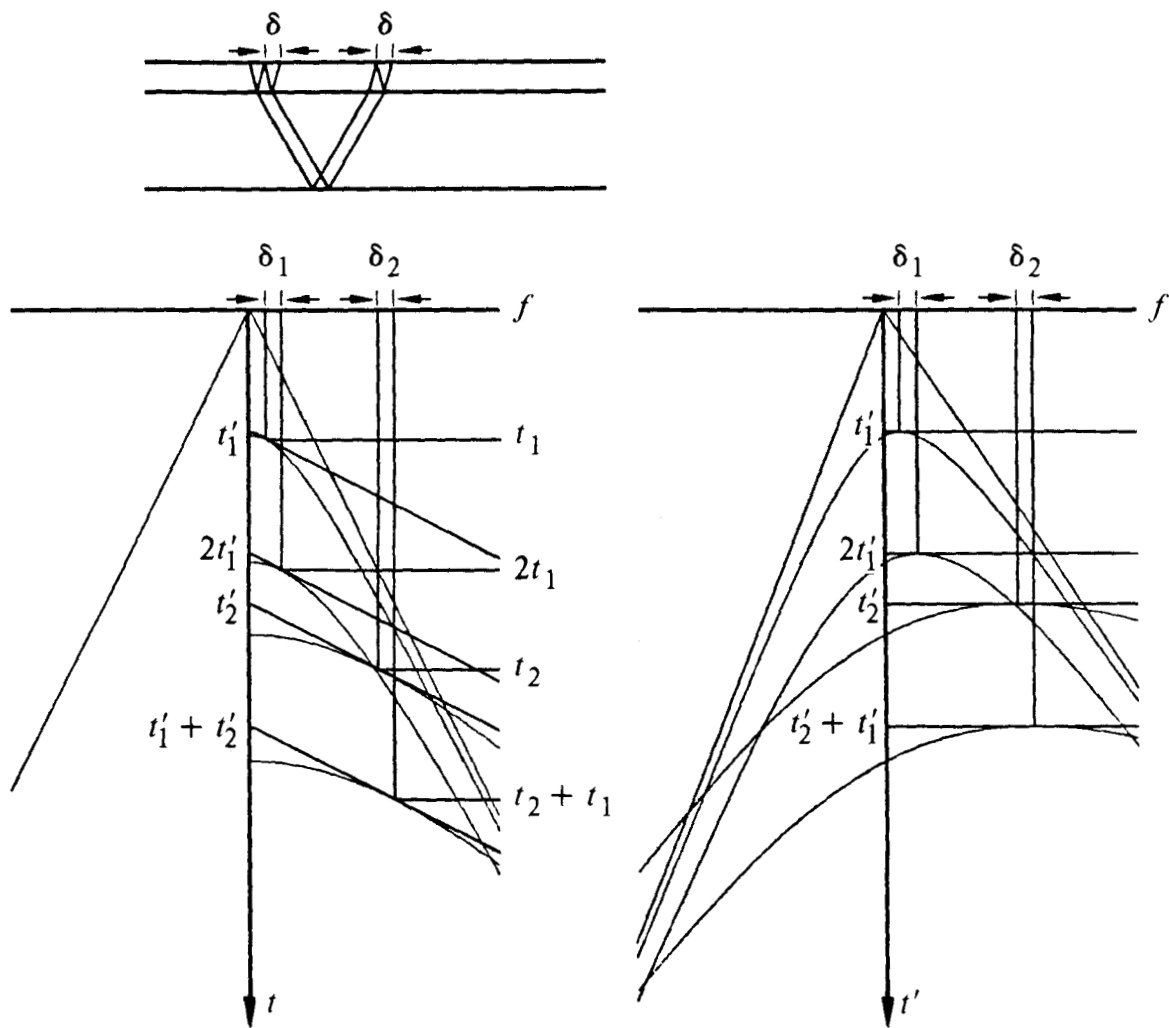


FIG. 5.6-2. A two-layer model showing the events $(t_1, 2t_1, t_2, t_2+t_1)$. On the top is a ray trace. On the left is the usual data gather. On the right the gather is replotted with linear moveout $t' = t - pf$. Plots were calculated with $(v_1, v_2, 1/p)$ in the proportion (1,2,3). Fixing our attention on the patches where data is tangent to lines of slope p , we see that the arrival times have the vertical-incidence relationships — that is, the reverberation period is fixed, and it is the same for simple multiples as it is for peglegs. This must be so because the ray trace at the top of the figure applies precisely to those patches of the data where $dt/dx = p$. Furthermore, since $\delta_1 = \delta_2$, the times $(t_1', 2t_1', t_2' + t_1')$ also follow the familiar vertical-incidence pattern. (Gonzalez)

where the hyperboloidal arrivals attain some particular numerical value of slope $p = dt/df$. These patches of energy seen on the surface observations each tell us where and when some ray of Snell's parameter p has hit the surface. Typical geometries and synthetic data are shown in figures 2 and 3.

Both the t_j and the t_j' behave like the times of normal-incident multiple reflections. While the lateral location of any patch unfortunately depends on the velocity model $v(z)$, slant stacking makes the lateral location irrelevant. In principle, slant stacking could be done for many separate values of p so that the (f, t) -space would get mapped into a (p, t) -space. The nice thing about (p, t) -space is that the multiple-suppression problem decouples into many separate one-dimensional problems, one for each p -value. Not only that, but the material velocity is not needed to solve these problems. It is up to you to select from the many published methods. After suppressing the multiples you inverse slant stack. Once back in (f, t) -space you could estimate velocity and further suppress multiples using your favorite stacking method.

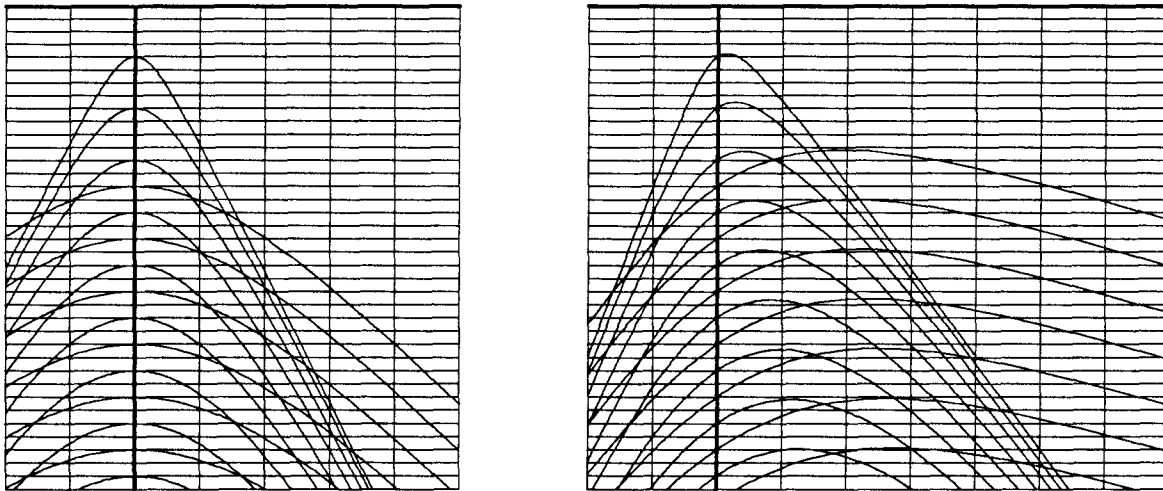


FIG. 5.6-3. The same geometry as figure 2 but with more multiple reflections.

Figure 3 is a “workbook” exercise. By picking the tops of all events on the right-hand frame and then connecting the picks with dashed lines, you should be able to verify that sea-bottom peglegs have the same interval velocity as the simple bottom multiples. The interval velocity of the sediment can be measured from the primaries. The sediment velocity can also be measured by connecting the n^{th} simple multiple with the n^{th} pegleg multiple.

Transformation to one dimension by slant stack for deconvolution is a process that lies on the border between experimental work and industrial practice. See for example Treitel et al [1982]. Its strength is that it correctly handles the angle-dependences that arise from the source-receiver geometry as well as the intrinsic angle-dependence of reflection coefficient. One of its weaknesses is that it assumes lateral homogeneity in the reverberating layer. Water is extremely homogeneous, but sediments at the water bottom can be quite inhomogeneous.

Near-Surface Inhomogeneity

Soils have strange acoustic behavior. Their seismic velocities are usually less than or equal to the speed of sound in water (1500 meters/sec). It is not uncommon for soil velocity to be five times slower than the speed of sound in water, or as slow as the speed of sound in air (300 meters/sec). Where practical, seismic sources are buried under the weathered zone, but the receivers are almost always on the surface. About the only time you may encounter buried receivers is in a marshy area. There field operations are so difficult that you will have many fewer receivers than normal.

A source of much difficulty is that soils are severely laterally inhomogeneous. It is not rare for two geophones separated by 10 meters to record quite different seismograms. In particular, the uphole transit time (the seismic travel time from the bottom of a shot hole to the surface near the top of the hole) can easily exhibit time anomalies of a full wavelength. All this despite a flat level surface. How can such severe, unpredictable, travel-time anomalies in the weathered zone be understood? By river meanders, tiny shallow gas pockets, pocketed carbonates, glacial tills, etc. All these irregularities can be found at depth too, but they are worse at the surface before saturation and the pressure of burial reduce the acoustic inhomogeneity. See also Section 3.7.

The shallow marine case is somewhat better. Ample opportunities for lateral variations still exist — there are buried submarine channels as well as buried fossil river channels. But the dominant aspect of the shallow marine case becomes the resonance in the water layer. The power spectrum of the observed data will be controlled by this resonance.

Likewise, with land data, the power spectrum often varies rapidly from one recording station to the next. These changes in spectrum may be interpreted as changes in the multiple reflections which stem from changes in the effective depth or character of the weathered zone.

Modeling Regimes

Downward-continuation equations contain four main ingredients: the slowness of the medium at the geophone $v(g)^{-1}$; likewise at the shot $v(s)^{-1}$; the stepout in offset space k_h/ω ; and the dip in midpoint space k_y/ω . These four ingredients all have the same physical dimensions, and modeling procedures can be categorized according to the numerical inequalities that are presumed to exist among the ingredients. One-dimensional work ignores three of the four — namely, dip, stepout, and the difference $v(g)^{-1} - v(s)^{-1}$. CMP slant stack includes the stepout k_h/ω . Now we have a choice as to whether to include the dip or the lateral velocity variation. The lateral velocity variation is often severe near the earth's surface where the peglegs live. Recall the simple idea that typical rays in the deep subsurface emerge steeply at a low-velocity surface. When using continuation equations in the near surface, we are particularly justified in neglecting dip, that is $v^{-1} \gg k_y/\omega$. It is nice to find this excuse to neglect dip since our field experiments are so poorly controlled in dip out of the plane of the experiment. Offset stepout, on the other hand, is probably always much larger in the plane of the survey line than out of it.

Another important ingredient for modeling or processing multiple reflections is the coupling of upcoming and downgoing waves. This coupling introduces the reflectivity beneath the shot $c(s)$ and the receiver $c(g)$. An important possibility, to which we will return, is that $c(s)$ may be different from $c(g)$, even though all the angles may be neglected.

Subtractive Removal of Multiple Reflections

Stacking may be thought of as a multiplicative process. Modeling leads to subtractive processes. The subtractive processes are a supplement to stacking, not an alternative: After subtracting, you can stack.

First we try to model the multiple reflections, then we try to subtract them from the data. In general, removal by subtraction is more hazardous than removal by multiplication. To be successful, subtraction requires a correct amplitude as well as a timing error of less than a quarter-wavelength.

Statistically determined empirical constants may be introduced to account for discrepancies between the modeling and reality. In statistics this is known as *regression*. For example, knowing that a collection of data points should fit a straight line, we can use the method of least-sum-squared-residuals to determine the best parameters for the line. A careful study of the data points might begin by removing the straight line, much as we intend to remove multiple reflections. Naturally an adjustable parameter can help

account for the difficulty expected in calculating the precise amplitude for the multiples. An unknown timing error is much harder to model. Because of the nonlinearity of the mathematics, a slightly different, more tractable approach is to take as adjustable parameters the coefficients in a convolution filter. Such a filter could represent any scale factor and time shift. It is tempting to use a time-variable filter to account for time-variable modeling errors. An inescapable difficulty with this is that a filter can represent a lot more than just scaling and amplitude. And the more adjustable parameters you use, the more the model will be able to fit the data, whether or not the model is genuinely related to the data.

The difficulty of subtracting multiple reflections is really just this: If an inadequate job is done of modeling the multiples — say, for example, of modeling the geometry or velocity — then you need many adjustable parameters in the regression. With many adjustable parameters, primary reflections get subtracted as well as multiples. Out goes the baby with the bath water.

Slanted Deconvolution and Inversion

Because of the wide offsets used in practice, it has become clear that seismologists must pay attention to differences in the sea floor from bounce to bounce. A straightforward and appealing method of doing so was introduced by Taner [1980] — that was his *radial-trace* method. A radial trace is a line cutting through a common-shot profile along some line of constant $r = h/t$. Instead of deconvolving a seismogram at constant offset, we deconvolve on a radial trace. The deconvolution can be generalized to a downward-continuation process. Downward continuation of a radial trace may be approximated by time shifting. Unfortunately, there is a problem when the data on the line consists of both sea-floor multiples and peglegs, because these require different trajectories. The problem is resolved, at least in principle, by means of Snell waves. Estevez, in his dissertation [1977], showed theoretically how Snell waves could also be used to resolve other difficulties, such as diffraction and lateral velocity variation (if known). An example illustrating the relevance of the differing depths of the sea floor on different bounces, is shown in figure 4.

Incompleteness of the data causes us to have problems with most inversion methods. Data can be incomplete in time, space, or in its spectrum. Any recursive method must be analyzed to ensure that an error made at shallow depths will not compound uncontrollably during descent. All data is spectrally incomplete. Also, with all data there is uncertainty about the shot waveform. At the p -values for which pegleg multiples are a problem, the first sea-floor bounce usually occurs too close to the ship to be properly recorded.

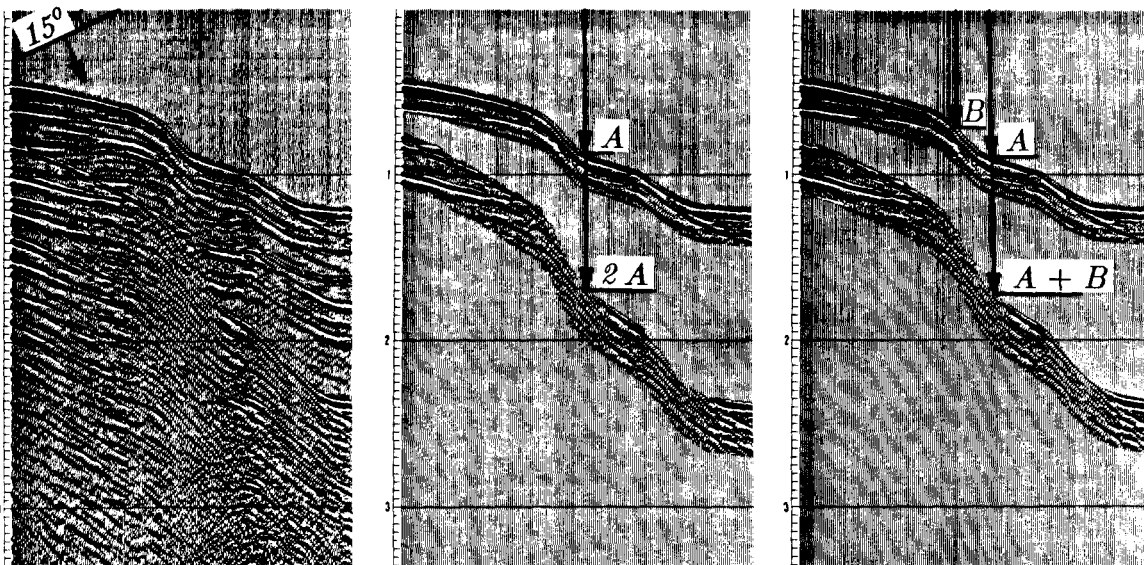


FIG. 5.6-4. Time of multiple depends on sum of all times. (Estevez [1977])

To solve this problem, Taner built a special auxiliary recording system.

It is an advantage for Snell wave methods that slant stacking creates some signal-to-noise enhancement from the raw field data, but it is a disadvantage that the downward continuation must continue to all depths. The methods to be discussed next are before-stack methods, but they do not require downward continuation much below the sea floor.

The Split Backus Filter

We are preparing a general strategy, *impedance replacement*, for dealing with surface multiple reflections. This strategy will require heavy artillery drawn from both regression theory and wave-extrapolation theory. So as not to lose sight of the goals, we will begin with an example drawn from an idealized geometry. That reality is not too far from this idealization was demonstrated by Larry Morley, whose doctoral dissertation [1982] illustrates a successful test of this method and describes the impedance-replacement strategy in more detail.

Imagine that the sea floor is flat. Near the shot the sea-floor reflection coefficient is taken as c_s . Near the geophone it is taken to be c_g . Near the geophone the reverberation pattern is

$$\frac{1}{1 + c_g Z} = 1 - c_g Z + c_g^2 Z^2 - c_g^3 Z^3 + c_g^4 Z^4 + \dots \quad (1)$$

where Z is the two-way delay operator for travel to the water bottom. (See Section 4.6 or FGDP for Z -transform background). Near the shot there is a similar reverberation sequence:

$$\frac{1}{1 + c_s Z} = 1 - c_s Z + c_s^2 Z^2 - c_s^3 Z^3 + c_s^4 Z^4 + \dots \quad (2)$$

Ignoring the difference between c_s and c_g leads to the Backus [1959] reverberation sequence, which is the product of (1) and (2):

$$\frac{1}{1 + c Z} \frac{1}{1 + c Z} = 1 - 2cZ + 3c^2 Z^2 - 4c^3 Z^3 + 5c^4 Z^4 + \dots \quad (3)$$

The denominator in (3) is the Backus filter. Applying this filter should remove the reverberation sequence. Morley called the filter which results from explicitly including the difference at the shot and geophone a *split Backus* filter. The depth as well as the reflection coefficient may vary laterally. (The effect of dip is second order). Thus the split Backus operator can be taken to be

$$(1 + c_s e^{i\omega\tau(s)}) (1 + c_g e^{i\omega\tau(g)}) \quad (4)$$

Inverting (4) into an expression like (3), you will find that the n^{th} term splits into n terms. This just means that paths with sea-floor bounces near the shot can have different travel times than paths with bounces near the geophone.

Figure 5, taken from Morley's dissertation, shows that split pegleg multiples are an observable phenomenon. His interpretation of the figure follows:

[The figure] is a constant-offset section (COS) from the same line for an offset halfway down the cable (a separation of 45 shot points with this geometry). The first-order pegleg multiple starting at 2.5 seconds on the left and running across to 3 seconds on the right is "degenerate" (unsplit) on the near-trace section but is split on the COS due to the sea-floor topography. The maximum split is some 200 mils around shot points 180-200. This occurs, as one might expect, where the sea floor has maximum dip; i.e., where the difference between sea-floor depths at the shot and geophone positions is greatest.

Most present processing ignores the Backus filter altogether and solves for an independent deconvolution filter for each seismic trace. This introduces a great number of free parameters. By comparison, a split Backus approach should do a better job of preserving primaries.

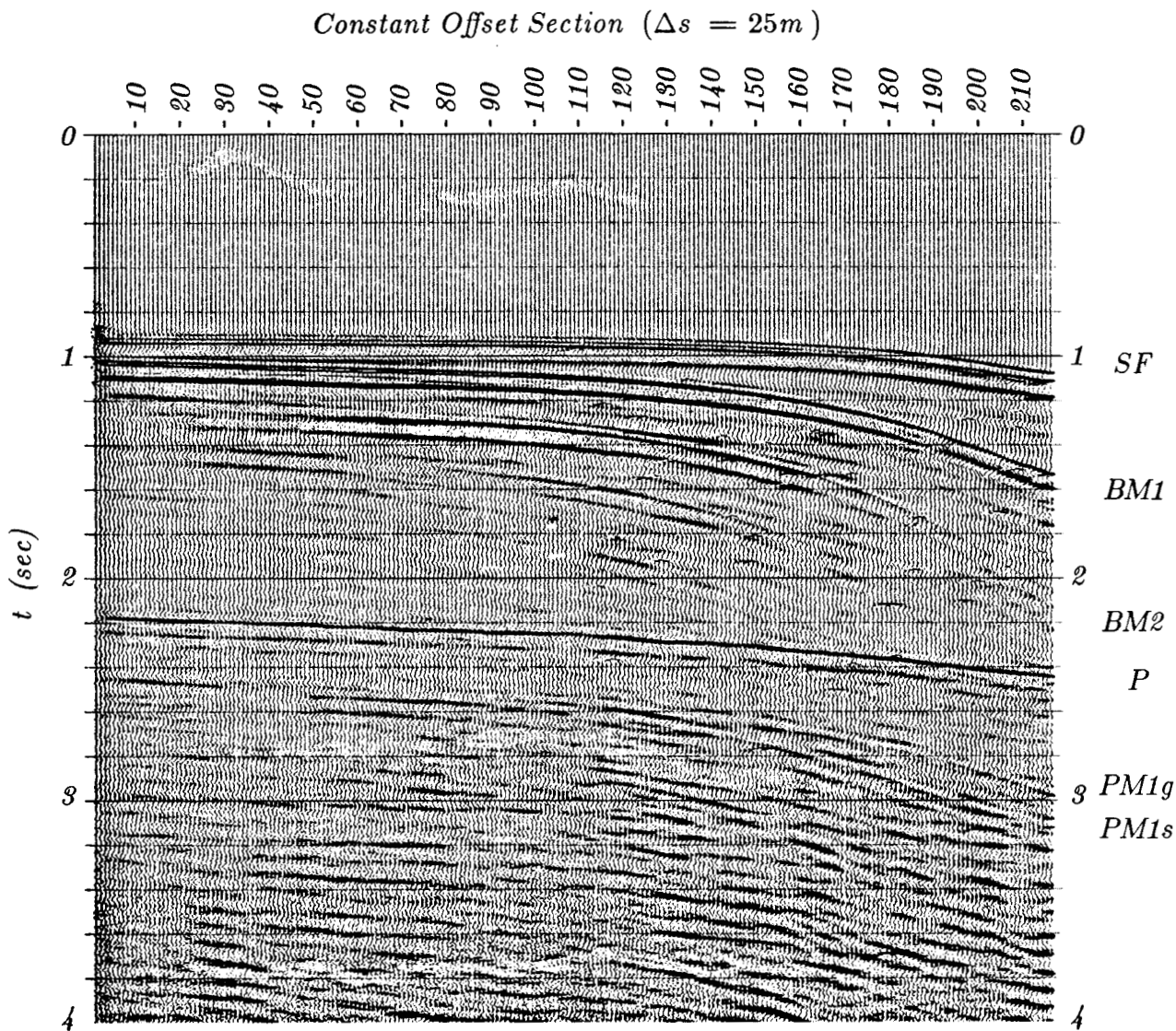


FIG. 5.6-5. Constant-offset section (COS) from the same line as figure 7 in Section 5.5. Offset distance is about 46 shotpoints. Notice that the first-order pegleg multiple is now split into two distinct arrivals, $PM1s$ and $PM1g$. (AMOCO Canada, Morley)

In practice we would expect that any method based on the split Backus concept would need to include the effect of moveout. Luckily, velocity contrast would reduce the emerging angle for peglegs. Of course, residual moveout problems would be much more troublesome with water-bottom multiples. Presumably the process should be applied after normal moveout in that case. Let us take a look at the task of estimating a split Backus operator.

Sea-Floor Consistent Multiple Suppression

Erratic time shifts from trace to trace have long been dealt with by the so-called surface-consistent statics model. Using this model you fit the observed time shifts, say, $t(s, g)$, to a regression model $t(s, g) \approx t_s(s) + t_g(g)$. The statistically determined functions $t_s(s)$ and $t_g(g)$ can be interpreted as being derived from altitude or velocity variations directly under the shot and geophone. Taner and Coburn [1980] introduced the closely related idea of a surface-consistent frequency response model that is part of the statics problem. We will be interpreting and generalizing that approach. Our intuitive model for the data $P(s, g, \omega)$ is

$$P(s, g, \omega) \approx \frac{1}{1 + c_s e^{i\omega\tau(s)}} \frac{1}{1 + c_g e^{i\omega\tau(g)}} \times \frac{i\omega}{v} \sqrt{z^2 + 4h^2} H(h, \omega) Y(y, \omega) F(\omega) \quad (5)$$

The first two factors represent the split Backus filter. The next factor is the normal moveout. The factor $H(h, \omega)$ is the residual moveout. The factor $Y(y, \omega)$ is the depth-dependent earth model beneath the midpoint y . The last factor $F(\omega)$ is some average filter that results from both the earth and the recording system.

One problem with the split Backus filter is a familiar one — that the time delays $\tau(s)$ and $\tau(g)$ enter the model in a nonlinear way. So to linearize it the model is generalized to

$$P'(s, g, \omega) \approx S(s, \omega) G(g, \omega) H(h, \omega) Y(y, \omega) F(\omega) \quad (6)$$

Now S contains all water reverberation effects characteristic of the shot location, including any erratic behavior of the gun itself. Likewise, receiver effects are embedded in G . Moveout correction was done to P , thereby defining P' .

Theoretically, taking logarithms gives a linear, additive model:

$$\ln P'(s, g, \omega) \approx \ln S(s, \omega) + \ln G(g, \omega) + \ln H(h, \omega) + \ln Y(y, \omega) + \ln F(\omega) \quad (7)$$

The phase of P' , which is the imaginary part of the logarithm, contains the *travel-time* information in the data. This information begins to lose meaning as the data consists of more than one arrival. The phase function becomes discontinuous, even though the data is well behaved. In practice, therefore, attention is restricted to the real part of (7), which is really a statement about power spectra. The decomposition (7) is a linear problem,

perhaps best solved by iteration because of the high dimensionality involved. In reconstructing S and G from power spectra, Morley used the Wiener-Levinson technique, explicitly forcing time-domain zeroes in the filters S and G to account for the water path. He omitted the explicit moveout correction in (5), which may account for the fact that he only used the inner half of the cable.

Replacement-Medium Concept of Multiple Suppression

In seismology wavelengths are so long that we tend to forget it is physically possible to have a directional wave source and a directional receiver. Suppose we had, or were somehow able to simulate, a source that radiated only down and a receiver that received only waves coming up. Then suppose that we were somehow able to downward continue this source and receiver beneath the sea floor. This would eliminate a wide class of multiple reflections. Sea-floor multiples and peglegs would be gone. That would be a major achievement. One minor problem would remain, however. The data might now lie along a line that would not be flat, but would follow the sea floor. So there would be a final step, an easy one, which would be to upward continue through a replacement medium that did not have the strong disruptive sea-floor reflection coefficient. The process just described would be called impedance replacement. It is analogous to using a replacement medium in gravity data reduction. It is also analogous to time shifting seismograms for some *replacement velocity*. (See Section 3.7).

The migration operation downward continues an upcoming wave. This is like downward continuing a geophone line in which the geophones can receive only upcoming waves. In reality, buried geophones see both upcoming and downgoing waves. The directionality of the source or receiver is built into the sign chosen for the square-root equation that is used to extrapolate the wavefield. With the reciprocal theorem, the shots could also be downward continued. Likewise shots physically radiate both up and down, but we can imagine shots that radiate either up or down, and mathematically the choice is a sign. So the results of four possible experiments at the sea floor, all possibilities of upward and downward directed shots and receivers, can be deduced.

Extrapolating all this information across the sea-floor boundary requires an estimate of the sea-floor reflection coefficient. This coefficient enters the calculation as a scaling factor in forming linear combinations of the waves above the sea floor. The idea behind the reflection-coefficient estimation can be expressed in two ways that are mathematically equivalent:

1. The waves impinging on the boundary from above and below should have a cross-correlation that vanishes at zero lag.
2. There should be minimum power in the wave that impinges on the boundary from below.

After the geophones are below, you must start to think about getting the shots below. To invoke reciprocity, it is necessary to invert the directionality of the shots and receivers. This is why it was necessary to include the auxiliary experiment of upward-directed shots and receivers.

EXERCISES

1. Refer to figure 3.
 - a. What graphical measurement shows that the interval velocity for simple sea-floor multiples equals the interval velocity for peglegs?
 - b. What graphical measurements determine the sediment velocity?
 - c. With respect to the velocity of water, deduce the numerical value of the (inverse) Snell parameter p .
 - d. Deduce the numerical ratio of the sediment velocity to the water velocity.
2. Consider the upcoming wave U observed over a layered medium of layer impedances given by (I_1, I_2, I_3, \dots) , and the upcoming wave U' at the surface of the medium (I_2, I_2, I_3, \dots) . Note that the top layer is changed.
 - a. Draw raypaths for some multiple reflections that are present in the first medium, but not in the second.
 - b. Presuming that you can find a mathematical process to convert the wave U to the wave U' , what multiples are removed from U' that would not be removed by the Backus operator?
 - c. Utilizing techniques in FGDP, chapter 8, derive an equation for U' in terms of U , I_1 , and I_2 that does not involve $I_3, I_4 \dots$.

5.7 Profile Imaging

A field profile consists of the seismograms of one shot and many receivers along a line. Migration of a single profile, or of many widely separated profiles, demands a conceptual basis that is far removed from anything discussed so far in this book, namely, exploding-reflector and survey-sinking concepts. Such a conceptual basis exists, predates (Claerbout [1970]), and seems more basic than that of exploding reflectors or survey sinking. I call this older imaging concept the *U/D* imaging concept.

The sinking concept seems to demand complete coverage in shot-geophone space. Exploding reflectors requires many closely spaced shots. On the other hand, profile imaging with the *U/D* concept has no requirement for density along the shot axis. An example of a dataset that could only be handled by the older concept is a sonobuoy. A sonobuoy is a hydrophone with a radio transmitter. It is thrown overboard, and a ship with an air gun sails away, repeatedly firing until the range is too great. The principle of reciprocity says that the data is equivalent to a single source with a *very* long line of geophones.

While improving technology is leading to greater sampling density on the geophone axis, we are unlikely to see increasing density in shot space. There are only twenty-four hours in a day, and we must wait ten seconds between shots for the echoes to die down. So, given a certain area to survey and a certain number of months to work, we end out with an irreducible shotpoint density. Indeed, with three-dimensional geometries proving their worth, we may see *less* spatial sampling density. Poor sample density in shot space is a small impediment to profile methods.

Unlike the exploding-reflector method and the survey-sinking method, *U/D* concepts readily incorporate modeling and analysis of multiple reflections. Indeed, an ingenious algorithm for simultaneous migration and de-reverberation is found in FGDP. In principle it can be applied to either field profiles or slant stacks.

Wave equation methods have been suggestive of new ways of making weathering-layer corrections. Yet none have yet become widely accepted in practice, and it is too early to tell whether a DSR approach or a profile approach will work better.

All these considerations warrant a review of the profile migration method and the *U/D* imaging concept. We could easily see a revival of these in

one form or another.

The U/D Imaging Concept

The U/D imaging concept says that *reflectors exist in the earth at places where the onset of the downgoing wave is time-coincident with an upcoming wave*. Figure 1 illustrates the concept.

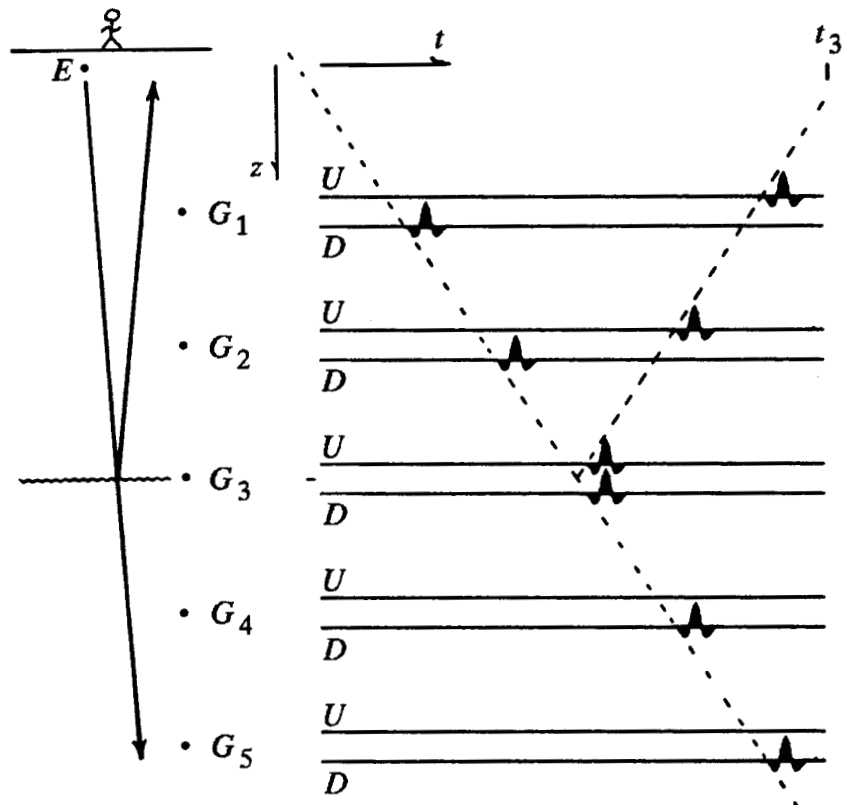


FIG. 5.7-1. Upcoming and downgoing waves observed with buried receivers. A disturbance leaves the surface at $t=0$ and is observed passing the buried receivers $G_1 \dots G_5$ at progressively later times. At the depth of a reflector, z_3 , the G_3 receiver records both the upcoming and downgoing waves in time coincidence. Shallower receivers also record both waves. Deeper receivers record only D . The fundamental principle of reflector mapping states that reflectors exist where U and D are time-coincident. (Riley)

It is easy to confuse the *survey-sinking* concept with the U/D concept because of the similarity of the phrases used to describe them: "downward continue the shots" sounds like "downward continue the downgoing wave." The first concept refers to computations involving only an upcoming wavefield $U(s, g, z, t)$. The second concept refers to computations involving both

upcoming $U(x, z, t)$ and downgoing $D(x, z, t)$ waves. No particular source location enters the U/D concept; the source could be a downgoing plane wave.

In profile migration methods, the downgoing wave is usually handled theoretically, typically as an impulse whose travel time is known analytically or by ray tracing. But this is not important: the downgoing wave could be handled the same way as the upcoming wave, by the Fourier or finite-difference methods described in previous chapters. The upcoming wave could be expressed in Cartesian coordinates, or in the moveout coordinate system to be described below.

The time coincidence of the downgoing and upcoming waves can be quantified in several ways. The most straightforward seems to be to look at the zero lag of the cross-correlation of the two waves. The image is created by displaying the zero-lagged cross-correlation everywhere in (x, z) -space.

The time coincidence of the upcoming wave and the earliest arrival of a downgoing wave gives evidence of the existence of a reflector, but in principle, more can be learned from the two waves. The amplitude ratio of the upcoming to the downgoing wave gives the reflection coefficient.

In the Fourier domain, the product $U(\omega, x, z)\bar{D}(\omega, x, z)$ represents the zero lag of the cross-correlation. The reflection coefficient ratio is given by $U(\omega, x, z)/D(\omega, x, z)$. This ratio has many difficulties. Not only may the denominator be zero, but it may have zeroes in the wrong part of the complex plane. This happens when the downgoing wave is causal but not minimum phase. (See Section 4.6 and FGDP). The phase of the complex conjugate of a complex number equals the phase of the inverse of the number. Thus the ratio U/D and the product $U\bar{D}$ both have the same phase. It seems you can invent other functional forms that compromise the theoretical appeal of U/D with the stability of $U\bar{D}$.

Don C. Riley [1974] proposed another form of the U/D principle, namely, that the upcoming waves must vanish for all time before the first arrival of the downgoing wave. Riley's form found use in wave-equation dereverberation.

Migration with Moveout Correction

If the earth were truly inhomogeneous in all three dimensions, we could hardly expect the data of a single seismic line to make any sense at all. But reflection seismology usually seems to work, even when it is restricted to a single line. This indicates that the layered model of the earth is a reasonable starting point. Thus normal-moveout correction is usually a good starting

process. Mathematically, NMO is an excellent tool for dealing with depth variation in velocity, but its utility drops in the presence of steep dip or a wide dip spectrum.

My early migration programs were based on concepts derived from single profiles. The data and the wave equation were transformed to a moveout-corrected coordinate system. This approach to migration is well suited to data that is sparsely sampled on the geophone axis. When steepness of dip becomes the ground on which migration is evaluated, then moveout correction offers little advantage; indeed, it introduces unneeded complexity. Whatever its merits or drawbacks, NMO commands our attention by its nearly universal use in the industrial world.

Moveout/Radial Coordinates in Geophone Space

Our theoretical analysis will abandon the geophone axis g in favor of a radial-like axis characterized by a Snell parameter p . (This really says nothing about the implied data processing itself, since it would be simple enough to transform final equations back to offset). The coordinate system being defined will be called a retarded, moveout-corrected, Snell trace, coordinate system. Ideal data in this coordinate system in a zero-dip earth is unchanged as it is downward continued. Hence the amount of work the differential equations have to do is proportional to the departure of the data from the ideal. Likewise the necessity for spatial sampling of the data increases in proportion to the departure of data from the ideal. Define

p	$(\sin \theta)/v$, the Snell ray parameter
t_p	any one-way time from the surface along a ray with parameter p
g	the surface separation of the shot from the geophone
t'	one-way time, surface to reflector, along a ray
τ	travel-time depth of buried geophones, one-way time along a ray
t	travel time seen by buried geophones
$v(p, t_p)$	a stratified velocity function $v'(z)$, in the new coordinates

The coordinate system is based on the following simple statements: (1) travel time from shot to geophone is twice the travel time from shot to reflector, less the time-depth of the geophone; and (2) the horizontal distance traveled by a ray is the time integral of $v \sin \theta = pv^2$; (3) the vertical distance traveled by a ray is computed the same way as the horizontal distance, but with a cosine instead of a sine.

$$t(t', p, \tau) = 2t' - \tau \quad (1)$$

$$g(t', p, \tau) = 2p \int_0^{t'} v(p, t_p)^2 dt_p - p \int_0^{\tau} v(p, t_p)^2 dt_p \quad (2)$$

$$z(t', p, \tau) = \int_0^{\tau} v(p, t_p) \sqrt{1 - p^2 v^2} dt_p \quad (3)$$

Surfaces of constant t' are reflections. Surfaces of constant p are rays. Surfaces of constant τ are datum levels. Unfortunately, it is impossible to invert the above system explicitly to get (t', p, τ) as a function of (t, g, z) . It is possible, however, to proceed analytically with the differentials. Form the Jacobian matrix

$$\begin{bmatrix} \partial_{t'} \\ \partial_p \\ \partial_{\tau} \end{bmatrix} = \begin{bmatrix} t_{t'}, g_{t'}, z_{t'} \\ t_p, g_p, z_p \\ t_{\tau}, g_{\tau}, z_{\tau} \end{bmatrix} \begin{bmatrix} \partial_t \\ \partial_g \\ \partial_z \end{bmatrix} \quad (4)$$

Performing differentiations only where they lead to obvious simplifications gives the transformation equation for Fourier variables:

$$\begin{bmatrix} -\omega' \\ k_p \\ k_{\tau} \end{bmatrix} = \begin{bmatrix} 2 & g_{t'} & 0 \\ 0 & g_p & z_p \\ -1 & g_{\tau} & z_{\tau} \end{bmatrix} \begin{bmatrix} -\omega \\ k_g \\ k_z \end{bmatrix} \quad (5)$$

It should be noted that (5) is a linear relation involving the Fourier variables, but the coefficients involve the original time and space variables. So (5) is in both domains at once. This is useful and valid so long as it is assumed that second derivatives neglect the derivatives of the coordinate frame itself. This assumption is often benign, amounting to something like spherical divergence correction.

Here we could get bogged down in detail, were we to continue to attack the nonzero offset case. Specializing to zero offset, namely, $p = 0$, we get

$$\begin{bmatrix} -\omega' \\ k_p \\ k_{\tau} \end{bmatrix} = \begin{bmatrix} 2 & 0 & 0 \\ 0 & 2t' - \tau & 0 \\ -1 & 0 & v \end{bmatrix} \begin{bmatrix} -\omega \\ k_g \\ k_z \end{bmatrix} \quad (6)$$

Equation (6) may be substituted into the single-square-root equation for downward continuing geophones, thereby transforming it to a retarded equation in the new coordinate system.

Historical Notes on a Mysterious Scale Factor

My first migrations of reflection seismic data with the wave equation were based on the U/D concept. The first wave-equation migration program was in the frequency domain and worked on synthetic profiles. Since people generally ignored such work I resolved to complete a realistic test on field data. Frequency-domain methods were deemed "academic." I found I could use the bilinear transformation of Z -transform analysis to convert the 15° wave equation to the time domain. As a practical matter, it was apparent that a profile migration program could be used on a section. But the theoretical justification was not easy. At that time I thought of the exploding-reflector concept as a curious analogy, not as a foundation for the derivation.

The actual procedure by which the first zero-offset section was migrated with finite differences was more circuitous and complicated than the procedure later introduced by Sherwood (Loewenthal et al [1976]) and adopted generally. The equation for profile migration in moveout-corrected coordinates has many terms. Neglecting all those with offset as a coefficient (since you are trying to migrate a zero-offset section), you are left with an equation that resembles the retarded, 15° extrapolation equation. But there is one difference. The $v \partial_{gg}$ term is scaled by a mysterious coefficient, $[t'/(2t'-\tau)]^2$. This is the equation I used. As the travel-time depth τ increases from zero to the stopping depth t' , the mystery coefficient increases slowly from $1/4$ to 1 .

Unfortunately my derivation was so complicated that few people followed it. (You notice that I do not fully include it here). My 1972 paper includes the derivation but by way of introduction it takes you through a conceptually simpler case, namely, the seismic section that results from a downgoing plane-wave source. This simpler case brings you quickly to the migration equation. But the mystery coefficient is absent. Averaged over depth the mystery coefficient averages to a half. (The coefficient multiplies the second x-derivative and arises from Δx decreasing as geophones descend along a coordinate ray path toward the shot). Sherwood telephoned me one day and challenged me to explain why the coefficient could not be replaced by its average value, $1/2$. I could give no practical reason, nor can I today. So he abandoned my convoluted derivation and adopted the exploding-reflector model as an assumption, thereby easily obtaining the required $1/2$. I felt more

comfortable about the mystery coefficient later when the survey-sinking concept emerged from my work with Doherty, Muir, and Clayton.

My first book, FGDP, describes how the U/D concept can be used to deal with the three problems of migration, velocity analysis, and multiple suppression. In only one of these three applications, namely, zero-offset migration (really CDP-stack migration), has the wave-equation methodology become a part of routine practice. None-the-less, the U/D concept has been generally forgotten and replaced by Sherwood's exploding-reflector concept.

5.8 Predictions for the Next Decade

In the 1960s seismologists learned how to apply time-series optimization theory to seismic data — see FGDP for that. Eventually time series reached the point of diminishing returns because its approach to spatial relations was oversimplified. In the 1970s seismologists learned to apply the wave equation. That's what this book has been about. You can see that the job of applying the wave equation is not yet complete, but we have come a long way. Perhaps we have solved most of our "first-order" problems, and the problems that remain are mainly "second order." For second-order effects to be significant, all the first-order phenomena must be reasonably accounted for.

Some first-order effects that this book has touched on only lightly relate to obvious, as well as subtle, imperfections in seismic data.

Problems in the Database

We often have a problem of *truncation*. The recording cable is of course finite in length, and perceptible waves generally travel well beyond it. The seismic survey itself has finite dimensions. We also have the problem of *gaps*. Gaps in seismic data may occur unpredictably, as when a gun misfires or surveyors are denied access to parcels of land in the midst of their survey. In addition we have the problem of spatial *aliasing*. Because of improving technology, we can expect a substantial reduction in aliasing on the geophone

axis, but aliasing on the shot axis will remain. There are only twenty-four hours in a day, and we must wait ten seconds between shots for the echoes to die down. So, given a certain area to survey and a certain number of months to survey it in, we end out with a certain number of shotpoints per square kilometer. With marine data, the spacing in the line of the path of the ship presents no problems compared to the problems presented by data spacing off the line.

Migration provides a mapping from a data space to a model space. This transformation is invertible (in the nonvanescent subspace). When data is missing, the transformation matrix gets broken into two parts. One part operates on the known data values, and the other part operates on the missing values. Except for a bit of Section 3.5, this book ignores the missing part. Although a strategy is presented in 3.5 for handling the missing part, it is very costly, and I believe it will ultimately be superseded or much improved.

Noisy data can be defined as data that doesn't fit our model. If the missing data were replaced by zeroes, for example, the data would be regarded as complete, but noisy. Data is missing where the signal-to-noise ratio is known to be zero. More general noise models are also relevant, but statistical treatment of partially coherent multidimensional wave *fields* is poorly developed in both theory and practice.

My prediction is that a major research activity of the next decade will be to try to learn to simultaneously handle both the physics and the statistics of wavefields.

Reuniting Optimization Theory and Wave Theory

Let's take a quick peek beyond this book into the future. A seismic image is typically a 1000×1000 plane, derived from a volume of about 1000^3 interrelated data points. There are unknowns present everywhere, not only in the earth model, but also in the data, as noise, as gaps, and as insufficient spatial density and extent of data recording. To assemble an interpretation we must combine principles from physics with principles from statistics. Presumably this could be done in some monster optimization formulation. A look at the theory of optimization shows that solution techniques converge in a number of iterations that is greater than the number of unknowns. Thus the solution to the problem, once we learn how to pose the problem properly, seems to require about a million times as much computing power as is available. What a problem!

But the more you look at the problem, the more interesting it becomes. First we have an optimization problem. Since we are constrained to make

only a few iterations, say, three, we must go as far as we can in those three steps. Now, not only do we have the original optimization problem, but we also have the new problem of solving it in an optimum way. First we have correlated randomness in the raw data. Then, during optimization, the earth model changes in a correlated random way from one iteration to the next. Not only is the second optimization problem the practical one — it is deeper at the theoretical level.

Throw Away Your Paper Sections.

Current seismic interpretation often amounts to taking colored pencils and enhancing aspects of a computer-generated image. Seismic interpretation is entering an era in which the interpretation will all be done on a video screen. The basic reason is that a sheet of paper is only two-dimensional, while most reflection data is three-dimensional. Modern 3-D surveys really record four-dimensional data. A video screen can show a movie. The operator/interpreter can interact with the movie. There are things I would like to show you, but I cannot show you in a book. Seismic data or even a blank sheet of paper has *texture*. When a textured object moves, you immediately recognize it. But I couldn't show it to you with pictures in this book. (Imagine a sequence of pictures of a blank sheet of paper, each one shifted some way from the previous one). The perception of small changes is blocked by any eye movement between pictures. Astronomers look for changes in the sky by rapidly blinking between looking at photographs taken at different times. Our eyes are special computers. Movies often show "where something comes from," enabling us to notice the unexpected in the general ambiance.

Most seismic interpretation is done on *stacked sections*. The original data is three-dimensional, but one dimension is removed by summation. Theoretically, the summation removes only redundancy while it enhances the signal-to-noise ratio. In reality, things are much more complicated. And much more will be perceptible when summations are done by the human eye (just by increasing the speed of a movie). There will be two generations of seismic interpreters — those who can interpret the prestacked data they see on their video screens — and those who interpret only stacked sections.